Interfacial Reaction of an Olefin-Terminated Self-Assembled Monolayer Exposed to Nitrogen Dioxide: An Investigation Into the Reaction Rate and Mechanism

Gwen M. Davis

Thesis submitted to the faculty of the Virginia Polytechnic Institute and State University in partial fulfillment of the requirements for the degree of

Master of Science

in

Chemistry

Dr. John R. Morris, Chair

Dr. T. Daniel Crawford

Dr. Mark R. Anderson

August 27, 2003

Blacksburg, Virginia

Keywords: self-assembled monolayers, unsaturated surface, reaction mechanism, nitrogen dioxide, ultrahigh vacuum

Interfacial Reaction of an Olefin-Terminated Self-Assembled Monolayer Exposed to Nitrogen Dioxide: An Investigation Into the Reaction Rate and Mechanism

Gwen M. Davis

Abstract

Reactions of strongly oxidizing pollutants with unsaturated hydrocarbon surfaces are important to many areas of scientific interest. For example, reactions of unsaturated hydrocarbons on the surface of tropospheric aerosols could have a great effect on the oxidizing capacity of the troposphere while the reaction products could be involved in the formation of clouds and smog. These reactions are also important in understanding the toxic effect inhalation of these pollutants have on the pulmonary surfactant of the lung, the only amicable air-water interface of the body. The fatty acids of this surfactant are as much as 30% unsaturated, and exposure to oxidizing pollutant is known to alter both the composition and function of the surfactant. Understanding the reaction mechanism will further the knowledge of how this toxicity occurs.

While the reactions of strongly oxidizing pollutants, such as ozone and nitrogen dioxide, with alkenes in the gas and solution phases are well known, the interfacial reaction mechanisms of these species is not fully understood. The goal of this study is to determine the reaction mechanism when an unsaturated hydrocarbon monolayer at the gas-surface interface is exposed to gas phase nitrogen dioxide.

An olefin-terminated thiol was synthesized and a self-assembled monolayer on Au(111) made and characterized using Reflection-Absorption Infrared Spectroscopy (RAIRS). This unsaturated surface was then exposed to NO_2 at a pressure of $1x10^{-4}$ mbar in a UHV (Ultrahigh Vacuum) chamber. Time-resolved RAIRS was preformed *in situ* to monitor the reaction during exposure. X-ray Photoelectron Spectroscopy and RAIRS determined the surface reaction product as an aldehyde. While the mechanism can not be precisely determined, two mechanisms involving either the hydrogen abstraction or radical addition of the NO_2 to yield an aldehyde are proposed.

Acknowledgements

There are several people to which I would like to extend my gratitude.

- Dr. John Morris for his advice, support and understanding that sometimes life takes a left turn.
- My committee members: Dr. Mark Anderson and Dr. Daniel Crawford.
- The Morris Group: Melinda Ferguson, Scott Day, James Lohr, Wesley Gordon, and Larry Fiegland, especially for their patience in helping me in the lab during my pregnancy.
- Paige Landry for her invaluable help during the summer of 2002.
- Dr. Dessy for his helpful discussions and along with his wife, Lee, for their encouragement.
- Finally, to my family for their love, support, and encouragement especially my husband, Paul, who has stood beside me and our son Jacob, whose smile and laughter make it all worth wild.

Table of Contents

List of Figures

List of Tables

Chapter 1

Introduction and Motivation

1.1 Background

Strongly oxidizing pollutants are present both in the stratosphere and troposphere regions of the earth's atmosphere. Stratospheric ozone is important in preventing UV radiation from reaching the earth. In the troposphere, ozone is a secondary pollutant that can be detrimental to life. Tropospheric nitrogen dioxide is usually found in much greater concentrations than ozone. Both play an important role in the oxidizing capacity of the troposphere. Other oxidizing pollutants found in the earth's atmosphere include hydrogen peroxide, superoxide, hydroxyl radical, and peroxynitrite.[1] Peroxynitrite is especially potent because of its ability to form the OH radical,[2,3] the atmosphere's main oxidant.[4]

The reactions of strongly oxidizing pollutants with alkenes are important to many areas of scientific interest. For example, tropospheric chemistry involves the gas-phase reactions of alkenes and oxidants. The major sources of tropospheric alkenes in urban areas include engine exhaust, gasoline and solvent vapors, and emissions from vegetation.[5] The oxidation products of these alkenes could play an important role in the formation of clouds and smog. Furthermore, these reactions may have a great effect on the oxidizing capacity of the troposphere by the destruction and formation of oxidants.[6]

Reactions of these oxidizing species with olefins at the air-water interface are also an important component of tropospheric chemistry. Organic carbon makes up 24% of the composition of atmospheric aerosols, second only to sulfates as the major component.[4]

On the surface of the particulates, unsaturated hydrocarbons provide reaction sites for oxidants, which could also change the oxidizing capacity of the troposphere.[7]

The pulmonary surfactant in the alveolar regions of the lung is the only amicable air-water interface of the body. As much as 30% of the fatty acids that compose the pulmonary surfactant are unsaturated.[8] Exposure to oxidizing pollutants has been known to alter the composition of the surfactant as well as its functions.[9-16] The products from the reactions of these oxidizing species with the unsaturated fatty acids may play a role in transmitting the toxicity to distant cells which the reactive species could not otherwise reach.[17,18]

Many *in vivo* studies have investigated the effects of exposure to oxidizing pollutants. Upon exposure of rats to ozone, the unsaturated phospholipid composition of the pulmonary surfactant decrease to 75% of the clean air control.[9] A similar study using isotopically labeled $^{18}O_3$ found ^{18}O incorporated into the lung lavage as well as in the nose and trachea.[10] The amount of saturated phospholipids of the pulmonary surfactant decreased when rats were exposed to 10 ppm nitrogen dioxide. Simultaneously, the unsaturated phospholipid concentration increased.[11] Hydrogen peroxide both reduces the synthesis of phospholipids[12] and enhances the degradation of lipids by other reactive species, affecting the composition of the pulmonary surfactant.[13]

The research presented here focuses on the reaction of nitrogen dioxide with olefins at the gas-surface interface. When studying any reaction mechanism at an interface, the question arises as to whether the mechanism will follow that of the gas phase, the condensed phase or some combination of the two.[19] Therefore, the following

section reviews the reactions of alkenes and nitrogen dioxide in the gas and solution phases.

1.2 Reactions of Nitrogen Dioxide with Alkenes

The reactions of nitrogen dioxide with simple alkenes and dienes in both the gas phase and in solution have been studied in great detail. There are two possible pathways for the reaction of NO_2 with these unsaturated hydrocarbons: radical addition and hydrogen abstraction. In general, researchers find that the concentration of NO_2 determines the addition to abstraction ratio.[20] Furthermore, it has been shown that the presence of molecular oxygen also has a great effect on the products formed [21] as well as on the reaction rates.[22] Either NO_2, its dimer, N_2O_4, or both could be responsible for the reactions taking place although it is difficult to determine experimentally.[23]

1.2.1 Solution Phase Mechanisms

In solution, the predominate reaction changes from radical addition to hydrogen abstraction as the concentration of NO_2 reaches the low parts-per-million range. Pryor attributes this to the fact that at low concentrations of NO_2, the addition equilibrium (Reaction 1.1) will reverse, thus decreasing the addition to abstraction ratio, and the irreversible hydrogen abstraction (Reaction 1.6) is observed. In the presence of oxygen, a radical trapping species, slightly more addition is observed at low concentrations of NO_2.[20] Abstraction of the α-hydrogen is still the dominate mechanism as the reversal of addition back to starting products (Reaction 1.1) is faster than the trapping by oxygen (Reaction 1.3).[24] At high concentrations of NO_2, the excess of this trapping species

(Reaction 1.2) makes addition the dominate mechanism.[20,23] Addition of a second NO_2 could add via the nitrogen or the oxygen resulting in a dinitro or nitronitrite, respectively (Reaction 1.2). The peroxy radical, formed when molecular oxygen adds to the alkyl radical (Reaction 1.3), can react further with NO_2 to form a peroxynitrate (Reaction 1.4).[24] Peroxynitrates are unstable and will decompose to form either a nitro nitrate or nitro ketone depending on the conditions (Reaction 1.5).[25,26]

Radical Addition Mechanism

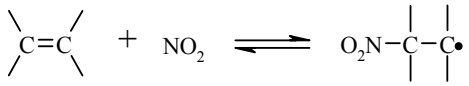

(1.1)

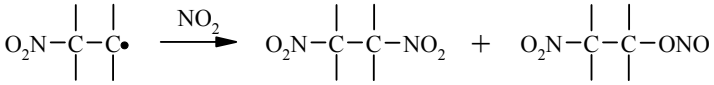

(1.2)

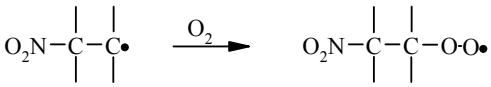

(1.3)

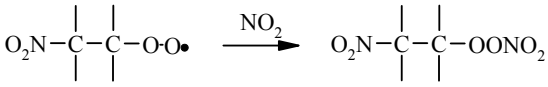

(1.4)

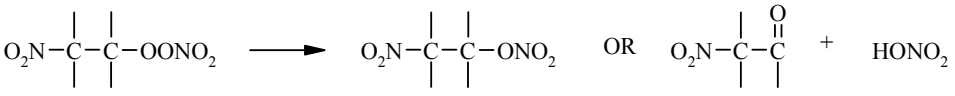

(1.5)

Hydrogen Abstraction Mechanism

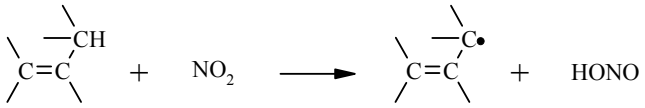

(1.6)

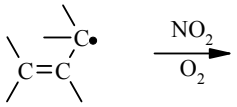

(1.7)

1.2.2 Gas Phase Mechanisms

In the gas phase, addition (Reaction 1.1) is the only process that has been observed.[27] Niki *et al*. performed their infrared study of the reaction of NO_2 with tetramethyl ethylene (TME) in the presence of air and oxygen.[22] The mixture of 1 Torr of both NO_2 and TME in 700 Torr of air produced the new absorption peaks listed in Table 1.1 for the peroxynitrate group.

Table 1.1 Infrared Frequencies for the Addition of NO_2 to alkenes

Functional group	Infrared band frequencies (cm^{-1})
Alkyl peroxynitrate	
R-$OONO_2$	1726, 1297, 788
Alkyl nitro	
R-NO_2	1560, 1383, 1350
Alkyl nitrate	
R-ONO_2	1675, 853

These three peaks start to appear after two minutes of exposure and are very prominate after 15 minutes when 9% of the TME has reacted. The other frequencies listed in Table

1.1 are seen in a residual spectrum in which peaks due to reactants have been subtracted out. These IR absorption peaks were also observed by Atkinson *et al*. in their study of alkenes and dialkenes with NO_2 in the gas phase.[28] A major product in the TME study was acetone, believed to be formed by the thermal dissociation of the nitro peroxy radical as seen in Reaction 1.8 and 1.9.[22]

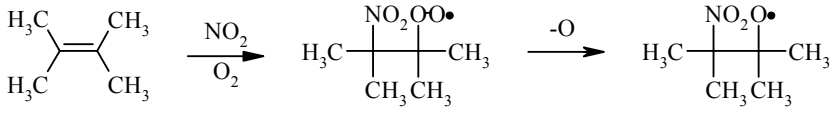

(1.8)

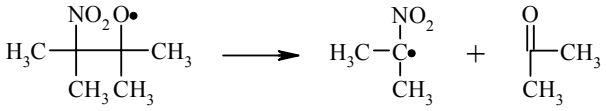

(1.9)

Nitrogen dioxide has also been know to catalyze the cis-trans isomerization of simple alkenes in the gas phase [27,29,30] and in solution[31] as well as unsaturated fatty acids in solution.[32] Addition of the NO_2 radical is followed by rotation of the carbon-carbon double bond and loss of NO_2 to yield the trans-isomer (Reaction 1.11).[30]

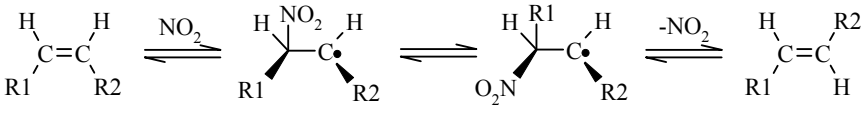

(1.11)

1.3 Self-Assembled Monolayers

Self-assembled monolayers (SAMs) are highly ordered molecular assemblies formed by the chemisorption of a surfactant-like molecule onto a substrate.[33] This chemisorption can be both ionic, as in the case of fatty acids on metal oxides,[34-37] or covalent, as organosulfur adsorbates assemble onto metals.[38-42] By changing the tail group to modify the chemical functionality of the surface, the potential applications of these monolayers are numerous.

Most commonly studied, alkanethiolates on Au(111) SAMs are especially appealing because of their high thermal stability,[43-46] well known packing density,[47-49] high structural order,[42] controllable surface chemical functionality,[47] and ease of preparation and analysis.[33] There are a variety of analytical methods that can be used to characterize these monolayers including elipsometry, contact angle measurements, cyclic voltammetry, X-ray photoelectron spectroscopy (XPS), and Reflection-Absorption Infrared spectroscopy (RAIRS).[33]

Alkanethiols have been shown to form densely packed, crystalline monolayers with an all trans conformation on Au(111) substrate.[39,40] The molecules bind to the gold substrate via a thiolate linkage and are tilted from the surface normal at an angle of 20-30°.[38] The crystalline structure of the individual SAMs are dependent on the thiol-Au interactions, van der Waals interactions between chains, and interactions of the end-groups.[47,50] The packing arrangement for the methyl-terminated SAM on Au(111) is well-established as a ($\sqrt{3}$ x $\sqrt{3}$)R30° based hexagonal overlay of the gold lattice.[48,51-54] It has been shown that the olefin-terminated monolayer studied here packs very similarly to the methyl-terminated monolayer.[55,56] Recent controversy over the interfacial structure

of the monolayer has ensued due to a X-ray diffraction study [57] in which the results pictured the molecules adsorbed as disulfides in a c(4x2) superlattice.[58,59] However, even more recent X-ray photoemission studies suggest that this disulfide component may just be a radiation-induced effect and surface degradation.[60,61]

1.4 Reactions in Monolayers

Due to their well-defined structure, low defect density, and chemical stability, SAMs provide a nearly ideal way to study reactions at an interface.[62] SAMs have been used in many areas of scientific interests including catalysis chemistry,[63] chemical sensing,[64,65] and electronics.[66] The ability to change the chemical and structural properties of these surfaces is important to the advancement of these applications.[67] Understanding surface reactions can also be applied to fundamental studies of chemistry and biochemistry.[68-70]

1.4.1 Steric Effects

Steric effects induced by the well packed alkane chains of the SAMs have been shown to have both favorable as well as adverse effects on interfacial reactions. In most cases, the high packing density hinders the penetration of reagents into the monolayer.[71-73] Kwon and Mrksich studied the steric effects on the Diels-Alder reaction of a self-assembled monolayer with buried quinone groups with solution phase dienes. They speculate that the enthalpic penalty that they observed is due to two reasons. First, the closely packed alkane chains prevent the optimal alignment and orientation of the impinging diene. Second, in order for the diene to enter the monolayer, the chains likely

have to undergo conformational changes, introducing gauche defects.[72] Fryxell *et al.* looked at S_N2 reactions of bromine-terminated monolayers. They concluded that the hydrocarbon matrix of the SAM sterically hindered the backside attack of the bromine group by the nucleophile while reactions that attacked the bromine directly were not affected.[71]

On the other hand, several studies have reported an acceleration of rates attributed to more favorable orientation of the reactive group in the monolayer.[74-77] For example, a Rh complex used as a catalyst for the hydrogenation of C=O bonds was found to have significantly enhanced activity when incorporated in a Langmuir-Blodgett film. Tollner *et al.* attributed this to the more favorable orientation of the Rh complex in the film.[77]

1.4.2 Reactions Starting at Defects

Schonherr *et al*. have developed a new microscopic approach to studying reaction kinetics on surfaces. With the reactants immobilized on an AFM tip, the pull-off forces with a inert surface were monitored as a function of time *in situ*, termed "inverted" chemical force microscopy by the group. This gives a sampling area of 10-100 molecules as opposed to 10^{12} molecules with RAIRS. Using this technique, they determined that for well-packed SAMs, reagents penetrate the monolayers at defect sites or domain boundaries. Reactions start at defect sites creating domains of reacted and unreacted molecules. The reaction proceeds at the boundaries of these domains until the entire monolayer is reacted.[78] This agrees with the hypothesis of others studying reactions in a monolayer.[71,79,80] Fryxell *et al*., reacting bromine- terminated monolayers to investigate nucleophilic displacements in SAMs, observed that as the reaction

approached 100% completion the rate slowed. They attributed this to the reaction starting at more accessible defect sites and then slowing down as the steric congestion increased.[71]

1.5 Reactions with Unsaturated Hydrocarbon Monolayers

Several studies involving the reactions of unsaturated hydrocarbon monolayers have been reported. Wasserman *et al.* looked at three reactions involving terminal olefin groups of alkyl-siloxane monolayers on silicon-silicon dioxide substrate. The olefin was oxidized to a carboxylic acid with $KMnO_4$ and $NaIO_4$. XPS and contact angle measurements confirmed that the reaction had taken place. The contact angle of water decreased from ~100° to ~30°; the surface had become more hydrophilic as the vinyl groups were converted to carboxylic acids. The contact angle for a carboxylic acid terminated alkanethiol SAM is 0º,[42] much lower than the reacted surface. Based on this, calculations determined that 80% of the surface was carboxylic acid. This does not distinguish, however, whether unreacted olefin groups or disordering of the monolayer, that had occurred during the reaction, was the cause for the difference in the contact angle.[81] This study had also been performed by Maoz and Sagiv on Langmuir-Blogget films with buried as well as terminal double bonds. They conclude that burying the double bond protects against oxidation by $KMnO_4$ as the oxidant can not penetrate into the monolayer. Any reaction that did occur was only at disordered defect site of the film.[82-84]

For many years, the Finlayson-Pitts group has studied unsaturated phospholipids at an interface, as a model for lung surfactant, and exposed them to reactive

gases.[19,21,85,86] The group has exposed phospholipids monolayers on a Langmuir trough to ozone.[19,85] Both surface and gas phase products were analyzed. The reaction appears to follow the well know mechanism for the ozonolysis of alkenes in solution;[87] acids and aldehydes remained on the surface [85] while a volatile aldehyde was released into the gas phase.[19]

The reactions of nitrogen oxides with phospholipids adsorbed onto glass cells have also been studied by the Finalyson-Pitts group.[21,86] Using High Performance Liquid Chromatography, Fourier Transfer Infrared Spectroscopy, and Fast Atom Bombardment Mass Spectrometry, the reactions products were determined after 1-palmitoyl-2-oleoyl-*sn*-glycero-phophocholine (POPC) was exposed to nitrogen dioxide. The reaction products depended heavily on the molar ratio of NO_2 to POPC. At low molar ratios, the only major product was 1-palmitoyl-2-elaidoyl-*sn*-glycero-phophocholine (PEPC), the trans-isomer of the starting phospholipids. The presence of oxygen did not affect the yield of PEPC, suggesting that the rotation of the C-C bond and the loss of NO_2 from the β-nitro alkyl radical, as seen in Reaction 1.11, occurs more rapidly than the scavenging by molecular oxygen or by NO_2 itself (Reactions 1.2 and 1.3). When the molar ratio was greater than or equal to 18, other products were observed, as well as PEPC, including the nitro alcohol, dinitro, nitronitrate, and the vinyl nitro. The fraction of these different products was also dependent on the presence of oxygen.[21]

1.6 Summary

The reactions of nitrogen dioxide with alkenes in the gas and solution phases are well know, but how these species will react in an organized monolayer has not been

studied in great detail. Despite the initial studies by Finlayson-Pitts, several questions still remain about the interfacial chemistry of this important class of reactions. Will the nitrogen dioxide be able to penetrate the monolayer in order to react with the double bond? Will the reaction proceed via the hydrogen abstraction or radical addition mechanism? What will the surface chemistry of the monolayer be after exposure to the oxidizing species? The following work was performed in hopes of further understanding the reaction mechanism upon the exposure of unsaturated hydrocarbon surfaces to NO_2. In the work presented here, self-assembled monolayers of olefin-terminated thiols were made and exposed to nitrogen dioxide. The reaction and its rate were probed using *in situ* reflection absorption infrared spectroscopy (RAIRS). RAIRS and X-ray Photoelectron Spectroscopy (XPS) then provided helped in determining reaction products.

Chapter 2

Instrumentation

2.1 Grazing Angle FTIR Spectrometer- Vacuum Chamber

In order to study reactions of surfaces exposed to reactive gases, we have developed an ultrahigh vacuum (UHV) chamber- FTIR system. The system enables *in situ* time-resolved FTIR studies of the surface reactions during exposure. Figure 2.1 shows a schematic of the Bruker IFS66v/S FTIR and UHV chamber set up.

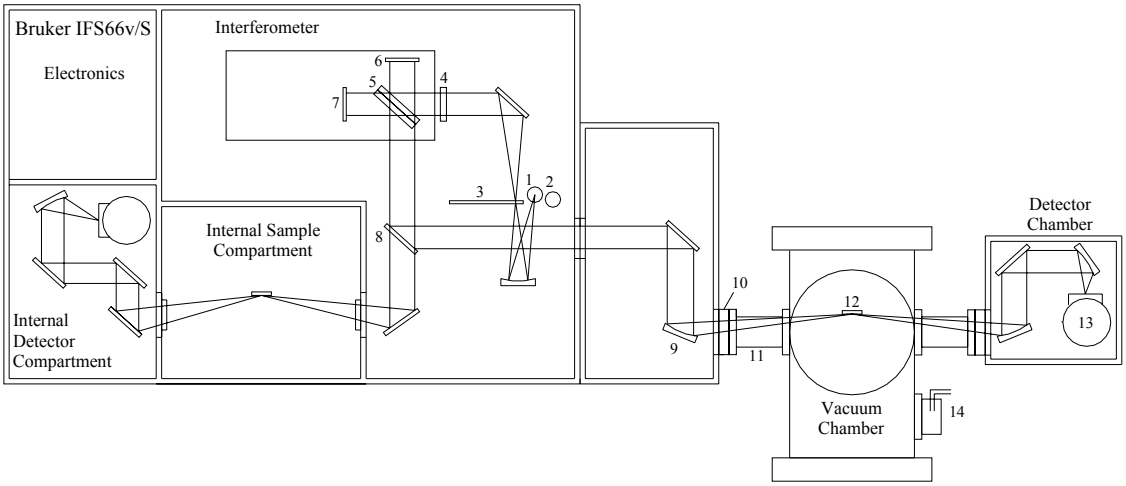

Figure 2.1 *In situ* RAIRS setup: (1) MIR source, (2) NIR/Vis source, (3) aperture wheel, (4) polarizer, (5) beam splitter, (6) fixed mirror, (7) scanning mirror, (8) movable mirror, (9) parabolic mirror, (10) KBr window, (11) bellows, (12) sample, (13) MCT detector, (14) leak valve.

The IR radiation from the SiC glowbar MIR source (no. 1) is focused onto the aperture wheel by a parabolic mirror (focal length 180 mm). This mirror will move to focus the light from either the glowbar or the Tungsten filament NIR/Vis source (no. 2), as selected by the user. The aperture wheel for these experiments has been set to the 0.7

mm × 4 mm aperture slit in order to maximize the spot size on the surface. Before entering the interferometer, the beam passes through a wire grid polarizer (no. 4), which selects the perpendicular component of the light. Once through the interferometer, the beam's direction is then determined by the movable mirror (no. 8). This mirror can be positioned so that the beam exits the spectrometer or proceeds into the internal sample compartment. In these experiments, the radiation was reflected into a separate mirror chamber where it was focused by a parabolic mirror (no. 9, focal length 250 mm) onto the sample. The angle of the beam with respect to the surface normal was approximately 83° and was set by moving the parabolic mirror (no. 9). After reflecting off the sample, the beam enters the external detector chamber and is focused by a parabolic mirror (focal length 250 mm), reflected from a flat mirror, and focused into the mercury-cadmium-telluride (MCT) detector by a second parabolic mirror (focal length 43 mm). The first parabolic mirror in the detector chamber was also moved in parallel with the exit mirror (no. 9) in the spectrometer. The instrument also has the option to collect spectra using the internal sample compartment. The movable mirror (no. 8) is rotated out of the way allowing the beam to be reflected into the internal sample compartment. A second MCT detector as well as a deuterated triglycine sulphate (DTGS) detector (not pictured) are available for analyzes in the internal detector chamber. The internal sample compartment is separated from the interferometer and detector compartment by KBr windows. This enables the sample compartment to be vented for sample introduction without venting the rest of the spectrometer. The internal sample set up was not used in the experiments presented here. The spectrometer and external detector chamber were kept under

vacuum, approximately 18 mbar, with a diaphragm pump (Vacuubrand, pumping speed 1.04 Ls^{-1}) to remove background gases such as water and carbon dioxide.

The UHV chamber is separated from the spectrometer and external detector chamber by KBr windows (no. 10, 55 mm $\phi \times 5$ mm, wedged 0.33°). These windows are housed in differentially pumped window flanges (McAllister) that give the option to pump the window separately. This was not necessary to achieve the desired pressure range for these experiments. The custom window flanges are connected to the UHV chamber via conflat flange flexible bellows (no. 11). An o-ring seals the connection between the spectrometer and the window flange.

The UHV sample chamber is pumped by a turbo molecular pump (Varian Model 969-9008, pumping speed 250 Ls^{-1}), which is equipped with a 6" gate valve. For introduction of the sample, the gate valve is closed and the chamber vented. Samples are introduced via a door on the front flange of the chamber. The slide is placed on the sample holder, which is mounted onto a manipulator (PHI model 10-504) that enables the translation of the surface in the x, y and z directions as well as manipulation of the rotation and tilt of the surface. When placing the surface onto the sample holder, it is important that the plane defined by the face of the slide be perpendicular to the plane of the beam. If this is not the case for either the background or sample slide, a sine wave will appear in the baseline of the spectrum. An example of such a spectrum is shown in Figure 2.2. In order to dampen vibrations of the manipulator during collection of spectra, an o-ring is held against the back of the sample holder by a linear translator on the back flange of the chamber.

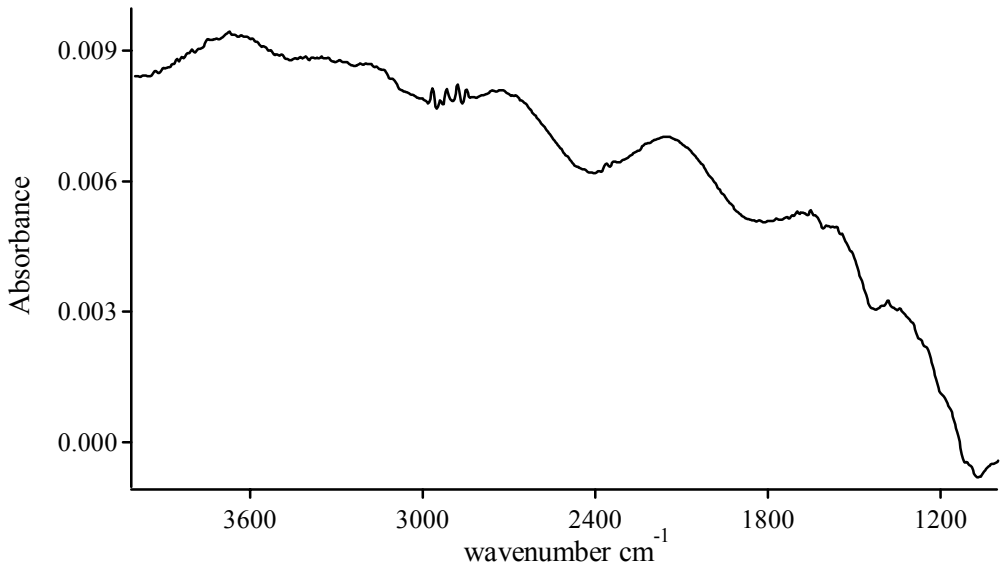

Figure 2.2: RAIRS spectrum of dodecanethiol. Sine wave in the background is due to misalignment of the slide on the sample holder.

When evacuating the chamber, a liquid nitrogen sorption pump is first used as a roughing pump. This evacuates the chamber to approximately 10^{-3} mbar at which time the gate valve is opened to the turbo pump. With the turbo pump, the pressure in the chamber will reach approximately 10^{-7} mbar. The chamber's base pressure is limited to 10^{-7} mbar due to o-ring seals on the chamber; with minor modification, the pressure is expected to reach ultrahigh vacuum conditions, P $<1x10^{-9}$ mbar. When the chamber is pumped down, the manipulator and sample move slightly thereby altering the amount of IR light reflected to the detector. Misalignment is corrected by adjusting the rotation of the sample until the amplitude of the interferogram is maximized. During these experiments, the amplitude was typically 10000.

The chamber is equipped with a variable precision leak valve (no. 14, MDC 315012) used to introduce reactive gases into the chamber. This valve allows for leaks as minute as $1x10^{-10}$ Torr ls^{-1}. The smallest leak noticeable to the experimental conditions

presented here, due to the pressure of the chamber and the precision of the pressure gauge (Pfeiffer Vacuum, Compact FullRange Gauge, PKR 251), is $1x10^{-8}$ Torr, corresponding to a 10^{-2} Langmuir s^{-1} exposure rate. A Langmuir is defined as the amount of time, at a given pressure, required to form one monolayer assuming a sticking probability of one. One Langmuir is equal to 10^{-6} Torr s.

2.2 Interlock Program

With any ultrahigh vacuum system, it is important to have an interlock system to protect the expensive instruments and pumps from pressure bursts and power loses. This system of switches and relays connected to a computer interface has been developed to operate a separate UHV molecular beam instrument in our laboratory. A similar system is under development for the FTIR-UHV system discussed here. The computer program, developed from LabView, monitors the pressures and checks them against user-selected set points. If the pressure in a certain chamber exceeds the set point, the program is set to close certain gates and valves to isolate the chamber and to turn off the pumps to that chamber. The program's front panel also allows the user to operate the gate valves, forlines and pumps as well as change the pressure set points from the computer. The following sections provide detail of the workings of the code. Figures of the LabView code can be found in the Appendix.

2.2.1 Reading Pressures

In the first sequence (Figure A.1), the program records the pressures in the main, detector, source, and load lock chambers as well as at the main/source forline and the

VHS 10 Diffusion pump forline via the main gauge controller (Pfeiffer Vacuum, Maxi Gauge, TPG 256A) into which the pressure gauges on the chambers are connected. The pressures are then displayed on the front panel (Figure 2.3). The sub vi "Read Press" communicates with the gauge controller; the string "PR#" refers to which sensor port on the controller the pressure gauge is connected.

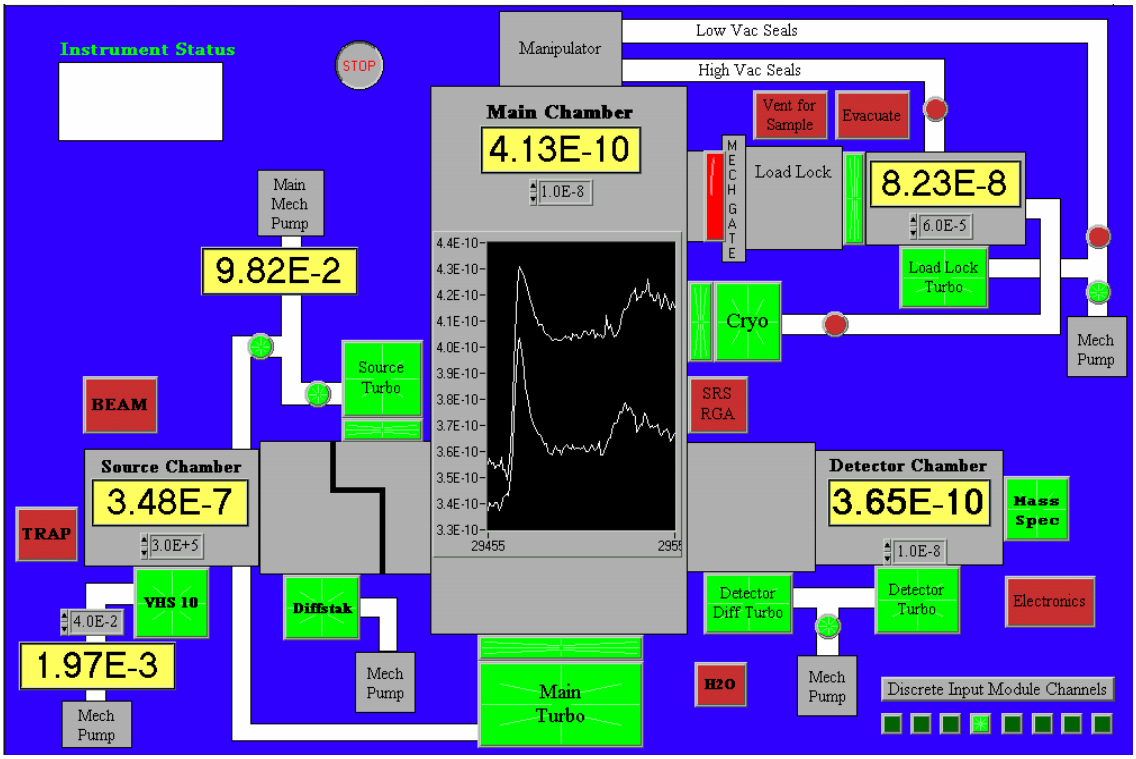

Figure 2.3: Front panel of the Interlock LabView program

The front panel displays a plot of the pressures in the main and detector chambers as a function of time. The program is set to display these pressures every 1000 times through the while loop which corresponds to about 15 minutes (Figure A.2). The graph is thus a twenty-four hour history of the pressures in these two chambers.

2.2.2 Pressure Set Points

When the program is started, the set points for the main chamber, detector chamber, source chamber and the VHS 10 Diffusion pump forline are set to the default values. After this, the set points can be changed from the front panel. For experiments in which corrosive or toxic gases are used, a liquid nitrogen trap is placed between the VHS 10 diffusion pump and its mechanical backing pump to prevent corrosion of the mechanical pump oil. The "Trap" Boolean on the front panel sets the source chamber and VHS 10 forline set points to high values to allow for installation of the liquid nitrogen trap (Figure A.3d). The "Beam" Boolean adjusts the set points in the source chambers for safe operation of the molecular beam (Figure A.3e). If neither of these Booleans is selected, the default values of the set points are used and manual control from the front panel is enabled. The set point for the load lock chamber is determined by the "Vent for Sample" and "Evacuate" Booleans (Figures A.4 and A.5) as discussed in the following section.

2.2.3 Load Lock Chamber

The UHV set-up is equipped with an auxiliary load lock chamber that allows for the introduction of a sample into the UHV chamber without venting. A sample is placed on the load lock translation stage and the load lock chamber evacuated. Once evacuated, a gate valve separating the load lock chamber from the main chamber is opened and the sample transferred onto the manipulator via the load lock arm. There are two Booleans that control the Load Lock chamber, "Vent for Sample" and "Evacuate". The "Vent for Sample" first changes the set point to a high value to allow for the vent (Figure A.4). The

program then closes the high vacuum seals, low vacuum seals, and cryo forline which all are connected to the load lock chamber. The load lock turbo is then turned off, its forline closed, and the chamber vented as the turbo pump slows down. The load lock gate remains open as the load lock chamber is vented through the turbo pump. Once the chamber is vented and the user turns off the "Vent for Sample" Boolean, the load lock set point reverts back to the default value and control of the set point from the front panel is again enabled.

Once the sample has been placed into the load lock chamber, the chamber must be evacuated for transfer of the sample into the main chamber. The "Evacuate" Boolean will again set the set point high so that pumps and valves can be opened while the pressure in the chamber is at atmosphere (Figure A.5). The load lock turbo is then turned on and its forline and gate are opened in order for the load lock chamber to be evacuated. The high vacuum seals, low vacuum seals, and cryo forline are left closed during the evacuation. Once the user turns off the "Evacuate" Boolean, the load lock set point is set back to the default and again control from the front panel is enabled.

2.2.4 Pressure Bursts

If a sudden increase in pressure occurs in a chamber, it is imperative to shut off all pumps to that chamber to avoid damage and to isolate the chamber from the rest of the system. For an example of how this is achieved, refer to Figure A.6 in the Appendix. First, the pressures in the source chamber and at the VHS 10 forline are checked against the set points. If either pressure is greater than its respective set point, the case will move to frame 1. In frame 1, the diffusion pumps are turned off. Frame 1 will always send the

case back to frame 0 so that the pressures are again checked. The process is repeated for the load lock chamber (Figure A.10) and the main and detector chambers (Figure A.9).

2.2.5 Cryo Pump

A power surge or interruption of cooling water may cause the cryo pump to turn off while the rest of the chamber remains in operation. With the cryo pump off and its gate open, the pressure in the main chamber will rise until it has gone above the main set point causing everything to be turned off. Rather than let this happen and the entire chamber vent, the cryo pump is first isolated from the main chamber. The cryo pump is given a set point of 0.5 times the main set point (Figure A.7). If the pressure in the main chamber goes above this cryo set point, the cryo pump is turned off and the cryo gate closed. If the problem is something more than the cryo pump, the pressure in the main chamber will continue to rise and everything will be turned off when the main pressure is checked against the main set point.

2.2.6 Mass Spectrometers and Electronics

The mass spectrometers and electronics have their own separate set points for the main and detector chamber pressures which are programmed directly into the base code (Figure A.8). This ensures that they can not be inadvertently turned on when the main and detector set points have been set high, for example when first evacuating the system. These set points are fixed in the program and cannot be changed from the front panel. It is also not necessary to change them in order to turn on the pumps when starting up.

2.2.7 Field Point Discrete Input Modules

Discrete input modules can be used to monitor the state, such as on/off or open/closed, of discrete devices, for example switches and relays. By monitoring the signal, such as voltage or current, from the device, the discrete input module indicates the state of the device. The LabView program must first read the status of the discrete input modules channels. (Figure A.11) The sub vi "DI-330 Read" reads the values for the DI-330 discrete input module's channels. The Boolean array of channels is then separated into the different Boolean indicators that appear on the front panel. These are just indicators and can not be changed by the user.

Currently, one discrete input channel is being used for an alarm system for the load lock's manual gate that separates the load lock from the main chamber. Catastrophic damage could occur if this gate valve was opened with the load lock chamber at atmospheric pressure. A magnetic reed contact switch on this manual gate is connected to one of the discrete input module channels. When the gate is closed, the switch is closed, and the discrete input is on. Opening the gate valve will in turn open the switch, which turns the discrete input off. When the discrete input is off, this signals the program to check the conditions of the load lock (Figure A.12). If the pressure in the chamber is below $1x10^{-5}$ mbar and the load lock gate is opened, it is safe to open the manual gate valve. If either of these two conditions is not met, the program will warn the user not to open the manual gate valve by abruptly closing the cryo gate. Once closed, a dialog box on the computer appears telling why the cryo gate has been closed and to close the manual load lock gate valve. The manual gate valve must be closed all the way so that the discrete input comes back on before closing the dialog box.

2.2.8 Field Point Relays

Power to all the pumps, valves, etc. on the chamber goes through field point relays in the interlock box. It is through these relays that the computer program controls the status of the pumps, valves, etc. The final frame of the program updates the values to the field point relay modules, which in turn will turn on or off the pumps, valves, etc (Figure A.13). The values for the Booleans are made into an array before being sent to the "FP-RLY 420" sub vi. The position on the array corresponds to the channel on the FP-RLY-420 relay modules. The string "FP-RLY-420@#" refers to the position of the relay modules on the Field Point Interface module.

The program "Field Point Explorer" is necessary to interface with the Field Point Modules. A file must be set up and saved in this program. The IAK outside of the while loop directs LabView to this file. Communication is then opened with the "FP Open" sub vi once every time the program is started. Once the program is stopped and taken out of the while loop, communication with the field point modules is closed with the "FP Close" sub vi.

Chapter 3

Nitrogen Dioxide Exposure of an Olefin-Terminated Monolayer

3.1 Introduction

The reactions of strongly oxidizing pollutants, such as nitrogen dioxide and ozone, with unsaturated hydrocarbons at an interface are important to many area of scientific interest. Organic carbon on the surface of atmospheric aerosols are potential reaction sites for these oxidiants.[7] These reactions could change the oxidizing capacity of the troposphere. Furthermore, the reaction products could have a role in the formation of clouds and smog.[6] At the only amicable air-water interface of the body, the fatty acids that compose the pulmonary surfactant in the alveolar regions of the lung are approximately 30% unsaturated.[8] Exposure to oxidizing pollutants has been known to alter the composition of this surfactant and in turn its functions.[9-16] The products from the reactions of these pollutants with the unsaturated fatty acids may play a role in transmitting the toxicity to distant cells which the initial reactive species could not otherwise reach.[17,18] Therefore, it is important to understand the reaction mechanism of oxidizing pollutants with unsaturated hydrocarbon surfaces.

The reactions of NO_2 with alkenes in the gas and condensed phases have been studied extensively over the past 60 years. There are two possible reaction mechanisms: radical addition and hydrogen abstraction. Both result in an alkyl radical that can further react with NO_2 or O_2.[20,23,24] These mechanisms are discussed in detail in Section 1.2.

While the reactions of nitrogen dioxides with alkenes in the gas and solution phases are well known, the interfacial reaction mechanism of these species is not fully understood. The goal of this study is to determine the reaction mechanism when an

unsaturated hydrocarbon monolayer at the gas-surface interface is exposed to gas phase nitrogen dioxide. There are many uncertainties about how this well know reaction will proceed when introduced to an ordered interfacial environment. Will the reaction proceed by the radical addition or hydrogen abstraction mechanism? Because of the many phases available at an interface, the reaction could be a combination of both the gas and solution mechanism.[19] How will the presence of oxygen affect the products? Once there is a radical on the surface, is it possible for this radical to react with a neighboring double bond, starting an oligimerization on the surface? Will the nitrogen dioxide instead react with the gold-sulfur bond thus removing the monolayer? Finally, will the reactive gas be able to penetrate the monolayer in order to react at all? The work presented here hopes to gain further insight into the answers to these questions.

3.2 Experimental

3.2.1 Synthesis of Olefin-Terminated Thiol

Undec-10-ene-1-thiol was synthesized using the thiourea route[88] as previously reported by Peanasky and McCarley.[55] In a three-neck round bottle flask equipped with a reflux condenser and bubbler, 100 mL of absolute ethanol was purged with ultra high purity argon for at least 40 minutes. To this, 25 mmoles of thiourea was added and the mixture stirred and purged with argon until the solid dissolved. Approximately 8-10 mmoles of undec-10-ene 1-bromide was slowly added with a syringe through a septum in the round bottle flask. The solution was heated to reflux using an oil bath with a temperature of 103°C and allowed to reflux for approximately 19 hours with constant argon purge. Thin-layer chromatography (TLC) and proton nuclear magnetic resonance (^{1}HNMR) spectroscopy were preformed to ensure that all bromide starting material had

been converted to the thiouronium salt (Reaction 3.1). Once the solution was cooled to room temperature, 10 mL of an aqueous 10% (w/w) solution of NaOH was added. The mixture was again heated to reflux for 4 hours with constant argon purge. Again, TLC and ^{1}HNMR were preformed to determine that all the thiouronium salt had been hydrolyzed (Reaction 3.2).

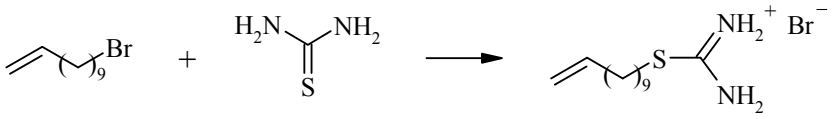

(3.1)

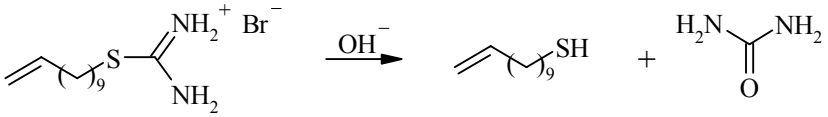

(3.2)

Once the solution cooled to room temperature, 20-25 mL of 1.2 M HCl was added until a pH of 7 was achieved. Before starting the extraction and purification steps, about 70% of the ethanol was removed. For the extraction, 200 mL of hexane was added and the bottom aqueous layer drained out of the separatory funnel. The remaining organic layer was washed three times with 20 mL of deionized water. The organic layer was then dried over anhydrous $MgSO_4$, filtered and the solvent removed under vacuum ($P \geq 0.1$ Torr). An oily product remained as well as a white solid, which may have been urea or excess thiourea. Hexane was used to pass the product through a silica gel column to remove the solid and purify the oil. Solvent was again removed under vacuum. A clear,

yellow oil was obtained and, as determined by ^{1}HNMR, the purity was 99% (Figure 3.1). The thiol was stored at 6°C.

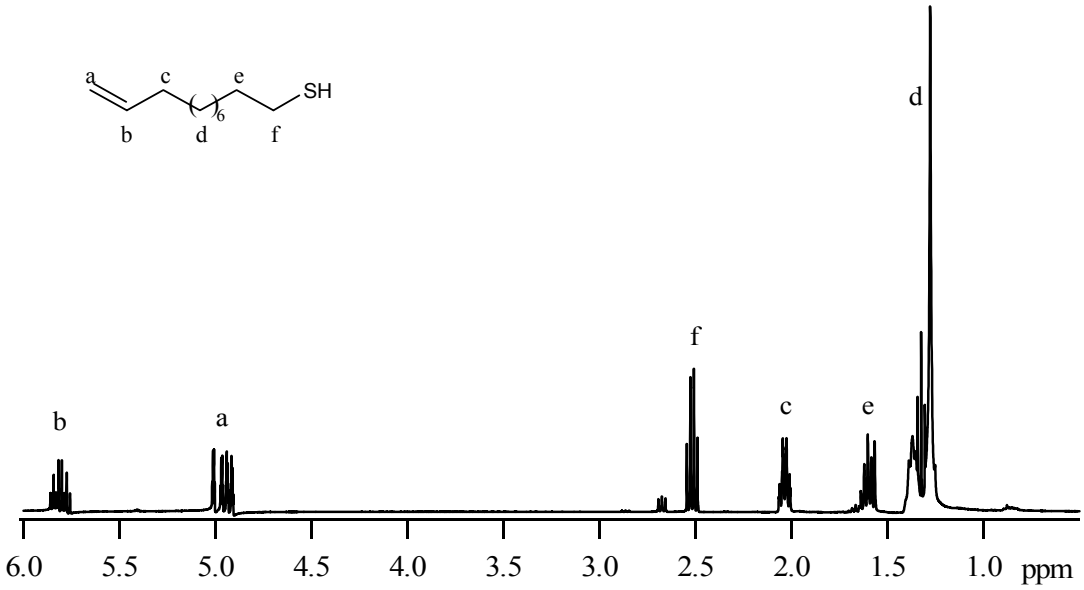

Figure 3.1: ^{1}HNMR of undec-10-ene-1-thiol

3.2.2 Preparation of Self-Assembled Monolayers

Monolayers were prepared on gold-coated glass slides (Evaporated Metal Films, Corp). These substrates consist of 1000 Å of Au with a 50 Å layer of Cr to adhere the Au to the glass. Gold slides were cleaned in a 30:70 H_2O_2/ H_2SO_4 piranha solution for one hour at room temperature. Slides were then rinsed in deionized water and absolute ethanol before being placed into the 1 mM ethanolic thiol solution. Thiol solutions were made of the aforementioned synthesized undec-10-ene-1-thiol, undecane-1-thiol (Aldrich, used as received), and a 60:40 saturated: unsaturated mixture of the two. Slides were left in the thiol solution for approximately 24 hours after which they were removed, rinsed with absolute ethanol, dried under a stream of ultra pure nitrogen, and stored in

petri dishes. Square inch slides for FTIR and square centimeter slides for XPS were made at the same time in the same jar for each of the three solutions.

3.2.3 Exposure of Monolayers to Nitrogen Dioxide

For the NO_2 exposure studies, two self-assembled monolayers were placed in the IR-vacuum chamber set up (Figure 2.1); one square inch slide placed in the sample holder for RAIRS measurements and one square centimeter slide placed on the bottom of the chamber to be used for post exposure XPS measurements. The chamber was then evacuated to a pressure of ~$3x10^{-6}$ mbar. A background of the sample was recorded before the NO_2 was introduced. The leak valve was then opened, allowing NO_2 into the chamber, until the pressure was ~$1x10^{-4}$ mbar. Exposures were done at pressures of $5x10^{-6}$, $1x10^{-5}$, and $5x10^{-5}$ mbar. No reaction was observed until the pressure was raised to $1x10^{-4}$ mbar. Once the NO_2 was introduced, the time-resolved study was started. The instrument was set to take a spectrum every 120 seconds for 60 minutes. At this pressure, no NO_2 gas phase IR peaks were observable. With the unreacted monolayer as the background, any peaks, negative or positive, in the spectra are indicative of changes in the structure or chemical nature of the surface. Once the exposure was complete, the leak valve was closed and NO_2 evacuated from the chamber. A spectrum was then collected of the remaining surface with a clean gold background. One clean gold background was collected in the morning and used throughout the day.

3.2.4 X-ray Photoelectron Spectroscopy

XPS measurements were preformed on the 1 cm^2 slides that had been in the chamber during exposure. Measurements were taken on a Perkin Elmer 5400 X-ray Photoelectron Spectrometer with a monochromatized Mg (Kα) radiation (1253.6 eV) source. Photoelectrons were analyzed at a take off angle of 15° with respect to the surface normal with a position sensitive multi-channel plate detector. Measurements were taken in an ultrahigh vacuum chamber with an approximate pressure of $1x10^{-7}$ mbar. The powerstat was set to 14 kV and 300 W and the pass energy was 44.75 eV for the surveys and 17.9 eV for the multiplexes. Multiplexes were taken for the C1s, O1s, N1s, Au4f, and Si2p regions with a total acquisition time of 25 minutes. For each multiplex the C1s peak was positioned at 285 eV by adjusting the anode energy. Adjusting the work function has the same result. This must be done to compensate for the surface charge induced by the gold.[89]

3.3 Results

3.3.1 Olefin-Terminated Self-Assembled Monolayer

RAIRS was used for the characterization of the olefin-terminated monolayer before exposure. Figure 3.2 shows the RAIRS spectrum of the self-assembled monolayer along with the spectrum of the neat alkenethiol liquid. Table 3.1 summarizes the important peaks in these two spectra.

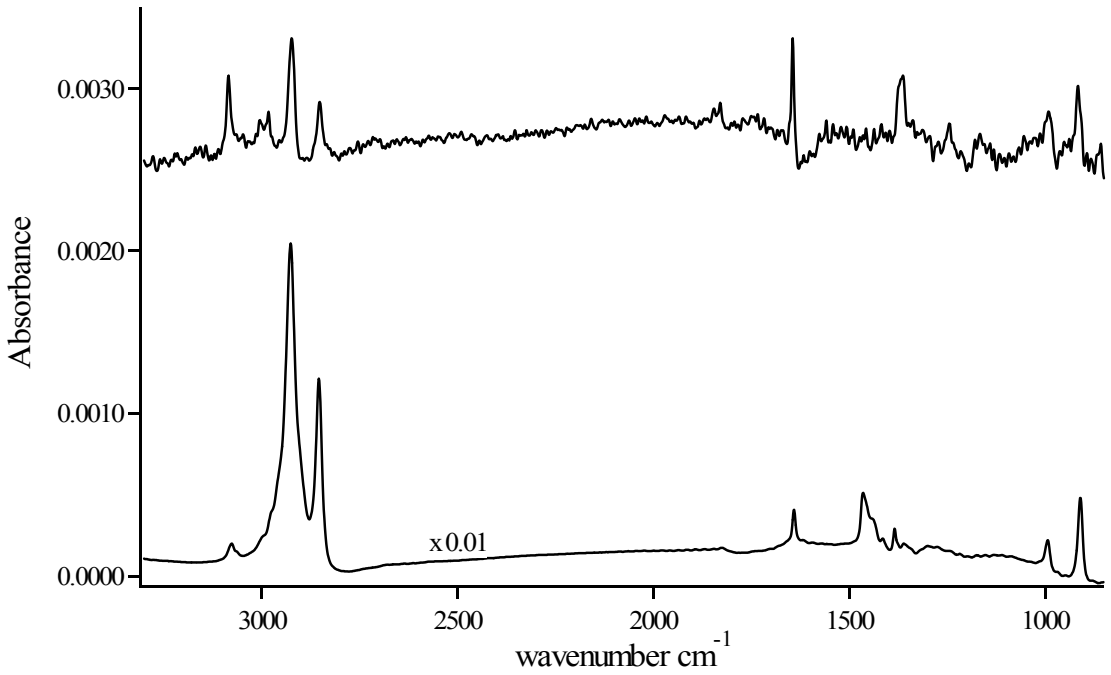

Figure 3.2: RAIRS spectra of olefin-terminated self-assembled monolayer (top) and the neat olefin thiol liquid (bottom).

Table 3.1: Infrared Peak Assignments for Olefin-terminated Monolayer

Peak Frequency (cm^{-1})		
Olefin-terminated SAM on Au(111)	Olefin-terminated thiol neat liquid	Vibration mode
3085	3077	$\nu_a(=CH_2)$
3005	Not observed	$\nu(H_2C=C-H)$
2983	Not observed	$\nu_s(=CH_2)$
2921	2926	$\nu_a(CH_2)$
2852	2854	$\nu_s(CH_2)$
1830	1826	$\omega(=CH_2)$ overtone
1644	1641	$\nu(C=C)$
991	993	C=C oop def
914	910	$\omega(=CH_2)$

There are seven peaks associated with the olefin group in the IR spectrum of the olefin-terminated SAM. Peaks at 3085 and 2983 cm^{-1} are due to the asymmetric and symmetric stretches, respectively, of the $=CH_2$ group while the peak at 3005 cm^{-1} is assigned to the $H_2C=C-H$ stretch. The peak at 3085 cm^{-1} has been blue shifted with

respect to the neat liquid spectrum. This is due to a change in the environment of the olefin group in the monolayer and has previously been reported to indicate a decrease in the hydrogen bonding of the double bond.[36,55] Although the more commonly observed effect of hydrogen bonding is a red shift in the vibrational frequency,[90] more recent studies report a blue shift in the C-H stretching vibrations from the formation of hydrogen bonds.[91,92] It is therefore difficult to say whether a decrease or increase in the hydrogen bonding of the double bond on the surface is causing the blue shift of the olefin peak.

Also observable in the spectrum are the peaks associated with the C=C stretch at 1644 cm^{-1}, the C=C out of plane deformation at 991 cm^{-1}, the out of plane deformation for the hydrogens in the $=CH_2$ group at 914 cm^{-1} and its overtone at 1830 cm^{-1}. Within the resolution of the spectra (±4 cm^{-1}), these peaks are identical for the SAM and the neat liquid. The peaks at 2921 and 2852 cm^{-1} correspond to the asymmetric and symmetric stretches, respectively, of the methylene groups in the chain. These peaks have been red shifted with respect to the neat liquid indicating that the molecules are in a more ordered environment on the surface.[38,93] This surface is not, however, as ordered and crystalline as most self-assembled monolayers of alkanethiols on Au(111) whose $\nu_a(CH_2)$ shifts to 2919 cm^{-1}.[39] The disorder in the olefin-terminated SAM may be due to gauche defect or incomplete surface coverage.[38] Additional peaks in the neat liquid spectrum between 1500 and 1350 cm^{-1} are associated with the scissoring of the methylene groups.[39]

3.3.2 Olefin-Terminated Monolayer Exposed to Nitrogen Dioxide

Figure 3.3 shows the time resolved study of the exposure of an olefin-terminated monolayer to NO_2. The unreacted monolayer is used as the background, so peaks in the spectra, negative or positive, are due to changes in the monolayer. After approximately four minutes, the olefin peak at 1644 cm^{-1} becomes negative indicating consumption of the double bond. After 12 minutes, the olefin peak at 3085 cm^{-1} is also negative, and a new positive peak at 2939 cm^{-1} is observed. A second peak at 2861 cm^{-1} appears after 18 minutes. The reaction was assumed to be complete after ~ 44 minutes based on the negative intensity of the olefin peak at 1644 cm^{-1} remaining constant. In the final spectrum of Figure 3.3, the olefin peaks at 1644 and 3085 cm^{-1} are negative while the new peaks have shifted to 2932 and 2858 cm^{-1}.

The flux of NO_2 onto the slide in the area defined by the spot size of the IR source (1 mm x 25.4 mm) was calculated to be 7.05×10^{16} molecules/s for the experimental pressure of 1×10^{-4} mbar. The concentration of olefin at the IR spot can be estimated as 10^{12} molecules. If all olefin groups reacted with NO_2, the reaction rate and rate constant were calculated as 3.70×10^{8} molecules/s and 1.94×10^{-24} molecules/s, respectively, based on the flux of NO_2 onto the surface and the 44 minute reaction time.

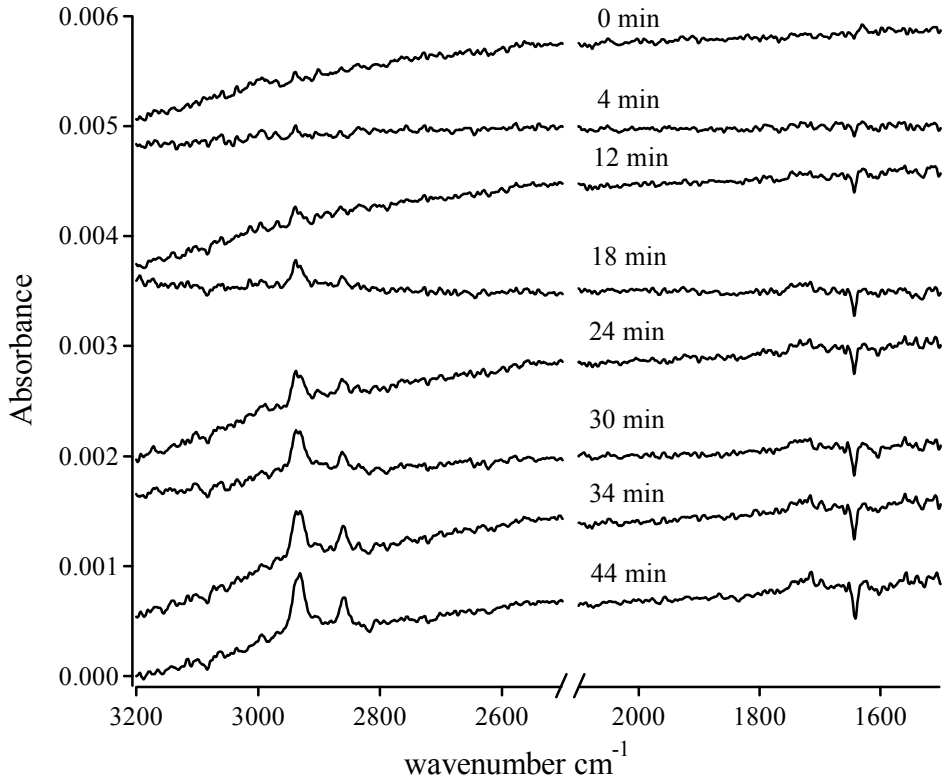

Figure 3.3: Time resolved RAIRS study of olefin-terminated monolayer exposed to NO_2

Figure 3.4 shows the RAIRS spectra of the olefin-terminated SAM before and after exposure to NO_2. The first observable change is the elimination of all peaks associated with the olefin. Secondly, the methylene peaks have been blue shifted to 2928 and 2856 cm^{-1} as well as increased in intensity by approximately two-fold. Finally, there are two new peaks at 2724 and 1734 cm^{-1}.

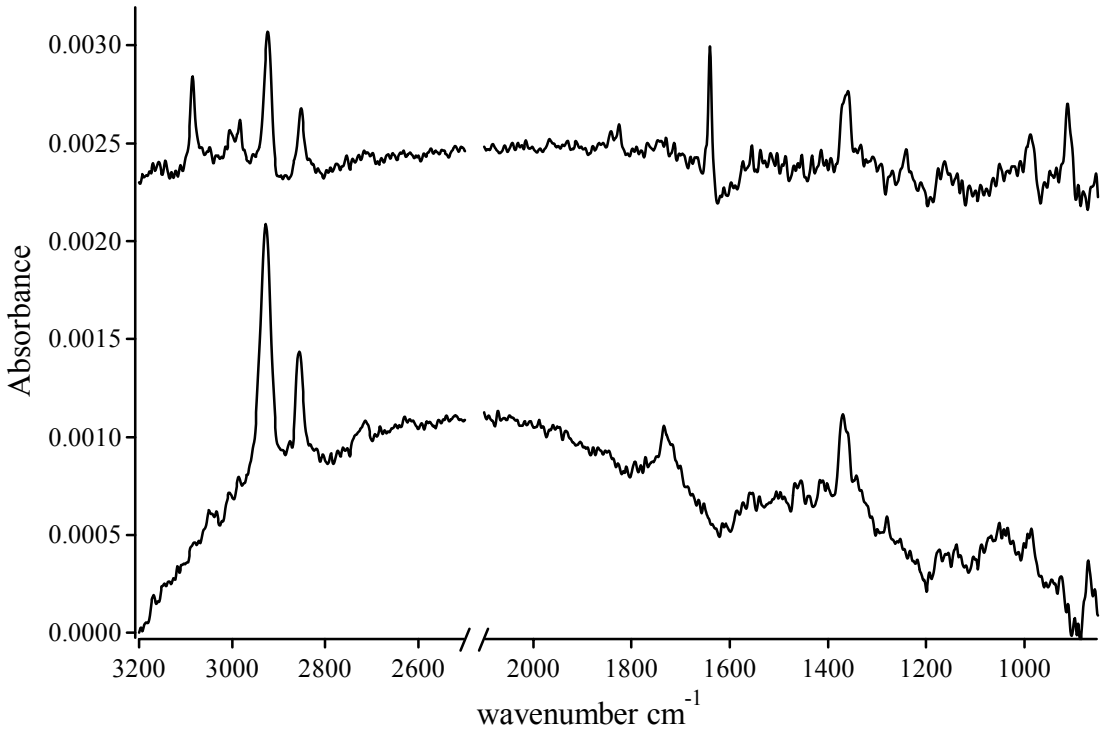

Figure 3.4: RAIRS spectrum of the olefin-terminated monolayer taken before (top) and after (bottom) exposure to NO_2

Within the signal-to-noise of this spectrum, it appears that the reaction has completely consumed the double bonds on the surface due to the elimination of the olefin peaks. The shift in the methylene peaks to higher frequencies indicates a disordering of the surface, while the increase in their intensities may be indicative of a reorientation of the chains resulting in their standing less upright.[55] For example, Porter *et al*. calculated that a change in the tilt angle from 30° to 35.4° would result in a 1.32 fold increase in the intensity of the methylene peaks.[38] Finally, peaks at 2724 and 1734 cm^{-1} are consistent with those observed for an aldehyde-terminated SAM. The peak at 1734 cm^{-1} is assigned to the C=O stretching mode while 2724 cm^{-1} is a Fermi resonance between the aldehyde C-H stretch and the first overtone of the C-H rocking vibration.[94]

3.3.3 NO_2 Exposure of Mixed Olefin/ Methyl and Methyl-Terminated Monolayers

Figure 3.5 shows the RAIRS spectra of the mixed olefin/methyl-terminated monolayer before and after exposure. In the top spectrum of Figure 3.5, the olefin peaks at 1644 and 3085 cm^{-1} are present. Based on the intensities of the peak at 1644 cm^{-1} for the mixed and 100% olefin-terminated monolayers, the mixed monolayer has an olefin concentration of ~20%. Also present in the spectra of Figure 3.5 are the peaks associated with the asymmetric and symmetric stretches of the methyl terminus group at 2966 and 2879 cm^{-1}, respectively. Based on the position of the methylene asymmetric stretch at 2923 cm^{-1}, this monolayer is even less well-ordered than the 100% olefin-terminated SAM.

The bottom spectrum of Figure 3.5 is the mixed monolayer after exposure to NO_2. Again, within the signal to noise, these spectra indicate that all of the olefin has been consumed. A new peak at 1734 cm^{-1} corresponding to the aldehyde is also present. The peaks assigned to the methyl and methylene stretches remained unchanged during the exposure. As a control, the 100% methyl-terminated monolayer was also exposure to NO_2. Upon exposure, the methyl-terminated monolayer did not change. No changes were observed in the methyl and methylene peaks and no presence of an aldehyde peak was detected.

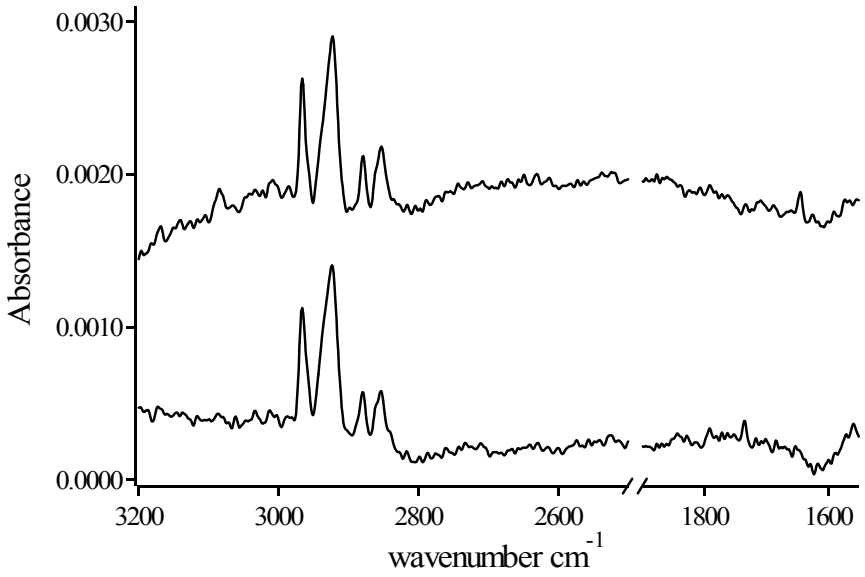

Figure 3.5: Mixed monolayer before (top) and after (bottom) exposure to NO_2

3.3.4 X-ray Photoelectron Spectroscopy Measurements

To further determine the surface chemistry after the exposure to NO_2, XPS measurements were taken of the olefin-terminated, methyl-terminated, and mixed monolayers. Shown in Figure 3.6 is the XPS survey of the olefin-terminated monolayer after exposure. Observable peaks correspond to the presence of oxygen, carbon, and gold. The presence of no other peaks is evidence that the surface is clean and has not been contaminated either before or after exposure. The absence of any silicon peaks from the glass substrate is indicates that the surface was in good aliment with the X-ray source during measurements. The same holds true for the methyl-terminated and mixed monolayers.

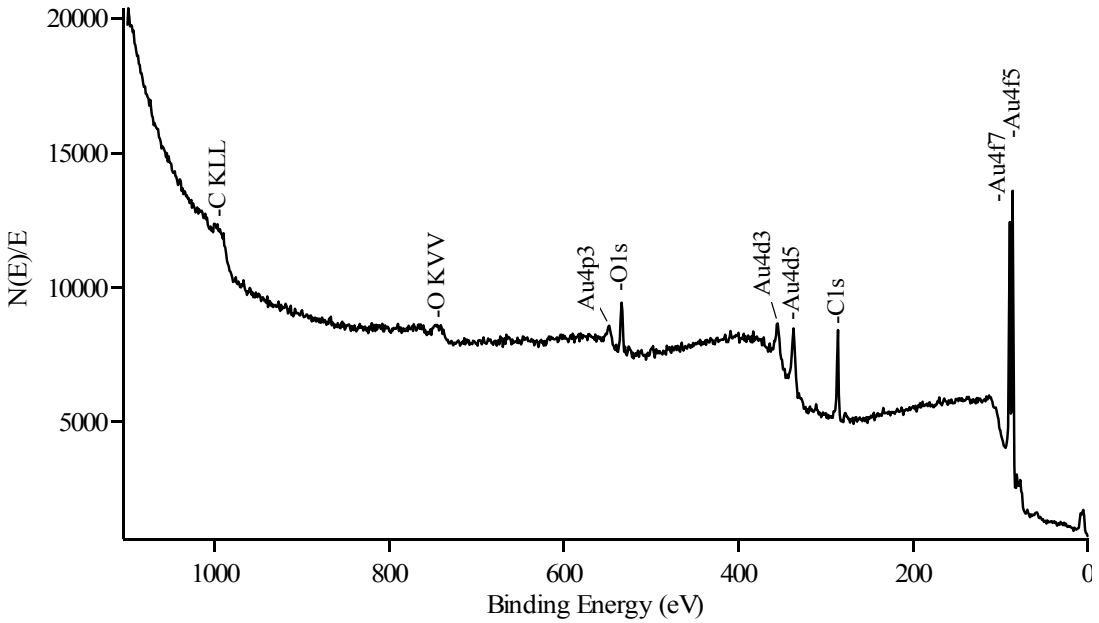

Figure 3.6: XPS survey of olefin-terminated SAM after exposure to NO_2

Multiplex measurements for the C1s, O1s, N1s, Au4f and Si2p regions were recorded. Figure 3.7 shows the C1s peak, which has been positioned at 285 eV. A second peak at 289 eV is also evident which corresponds to a carboxyl group. This is further evidence for the formation of an aldehyde in the reaction between the olefin and NO_2. It should be noted that the carbon-carbon double bond does not have a measurable shift in the XPS spectrum. This carboxyl shoulder is also present in the C1s multiplex of the mixed monolayer but not in the methyl-terminated monolayer. An oxygen 1s peak also emerges at 532.2 eV. This peak position corresponds to a carboxyl group (Figure 3.8).

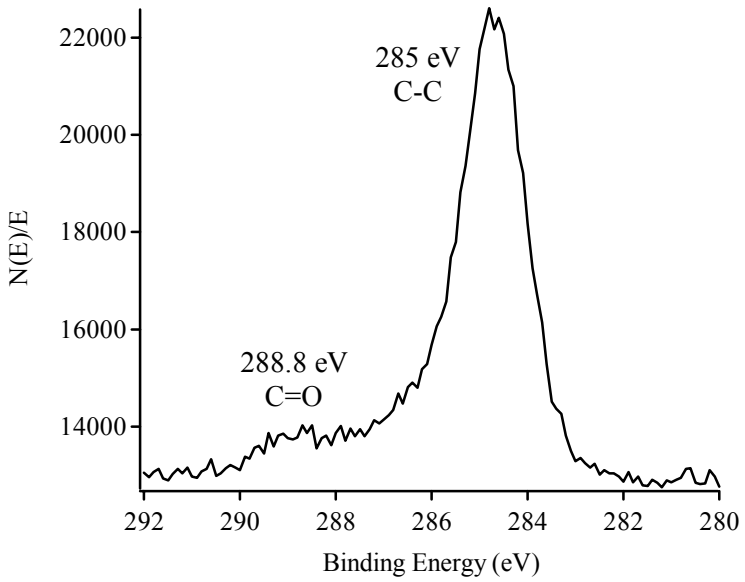

Figure 3.7: XPS C1s peak of the exposed olefin-terminated monolayer

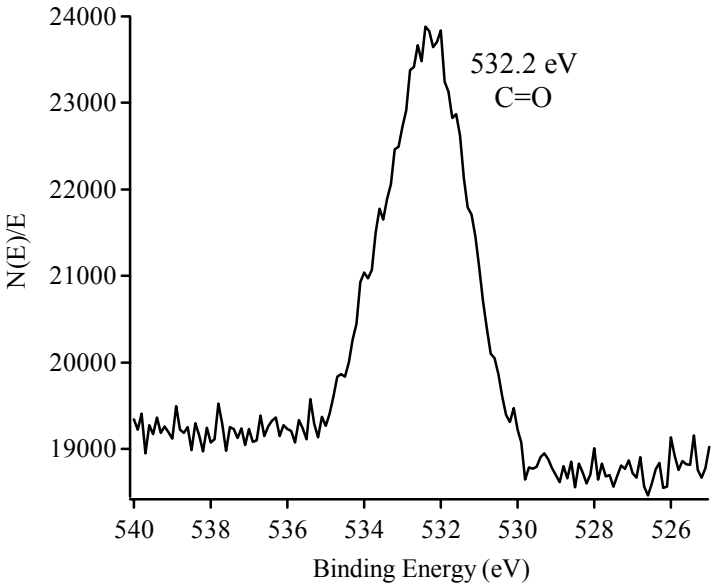

Figure 3.8: XPS O1s peak of the exposed olefin-terminated monolayer

3.4 Possible Mechanism for the Reaction of NO_2 with an Olefin-Terminated SAM

3.4.1 Via Hydrogen Abstraction

Kim *et al.* detected the presence of aldehydes and hydroxyl groups on the surface after exposing an olefin-terminated siloxane monolayer to X-rays in the presence of air. They propose that after removal of a hydrogen during irradiation, the remaining free radical reacts with oxygen to form the peroxy radical. The peroxy radical is unstable and known to decompose into alcohols, aldehydes and carboxylic acids.[95]

Hydrogen abstraction by nitrogen dioxide, although not know to happen in the gas phase, has been reported in solution. Figure 3.9 shows a possible mechanism for the formation of aldehydes upon hydrogen abstraction by NO_2 based on the X-ray exposure study done by Kim *et al*. After abstraction of the hydrogen, the alkyl radical would then react with oxygen in the chamber to form the peroxy radical. At the experimental pressure of $1x10^{-7}$ mbar presented here, the partial pressure of oxygen is approximately 10^{-8} mbar. The peroxy radical is unstable and will decompose to form the aldehyde.

Kim *et al*. see this transformation in both the methyl-terminated and the olefin-terminated monolayers upon exposure to X-rays.[95] Although hydrogen abstraction of alkanes has been know to occur, the reaction is endothermic and slow, occurring only at very high temperatures.[96] For the room temperature conditions of this NO_2 exposure experiment, this should not occur for the methyl-terminated monolayer and no aldehyde detected.

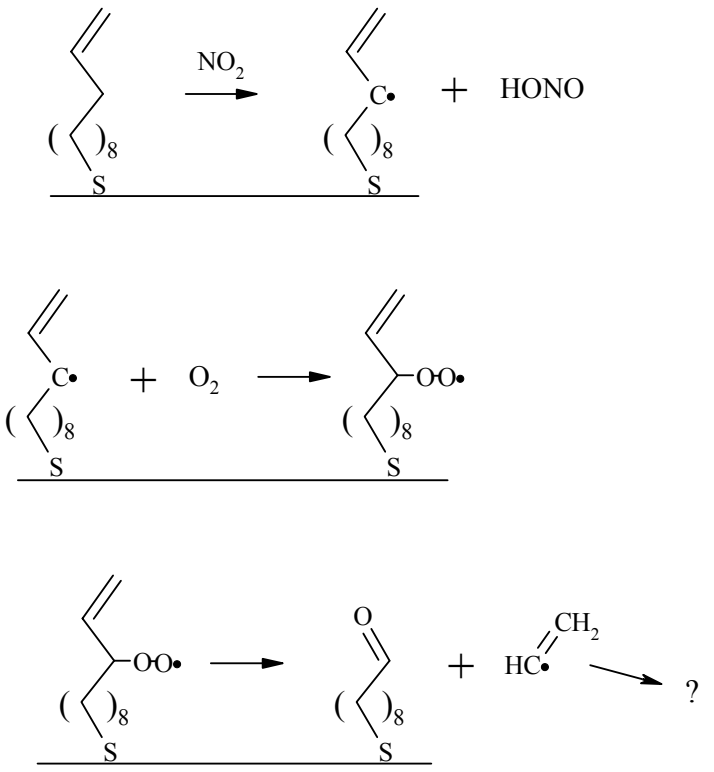

Figure 3.9: Formation of an aldehyde-terminated monolayer via hydrogen abstraction by NO_2 of an olefin-terminated monolayer.

3.4.2 Via Radical Addition

The formation of carboxyl groups via the addition of nitrogen dioxide to an olefin group has been documented both in the gas phase [22] and in solution.[24-26] Figure 3.10 shows a proposed mechanism for the addition of NO_2 to the olefin-terminated monolayer to yield an aldehyde-terminated monolayer based on the gas phase work done by Niki *et al.*.[22] Nitrogen dioxide adds to the double bond to form an alkyl radical on the surface. When adding to the double bond, the NO_2 will always attach to the carbon with the most hydrogens.[26] This radical then reacts with oxygen to form the nitro peroxy radical. As mentioned before, the peroxy radical is unstable and will decompose into the aldehyde

and nitro alkyl radical. In further reactions with NO_2 and O_2, the NO_2-CH_2 racial will form NO_2 and the corresponding carboxyl group, in this case formaldehyde.[22] Further gas-surface experiments could include investigating the presence of formaldehyde as a gas phase byproduct of this surface reaction. Addition of NO_2 to alkanes has also been know to occur but again only at very high temperatures and therefore should not occur at the conditions presented here.[96]

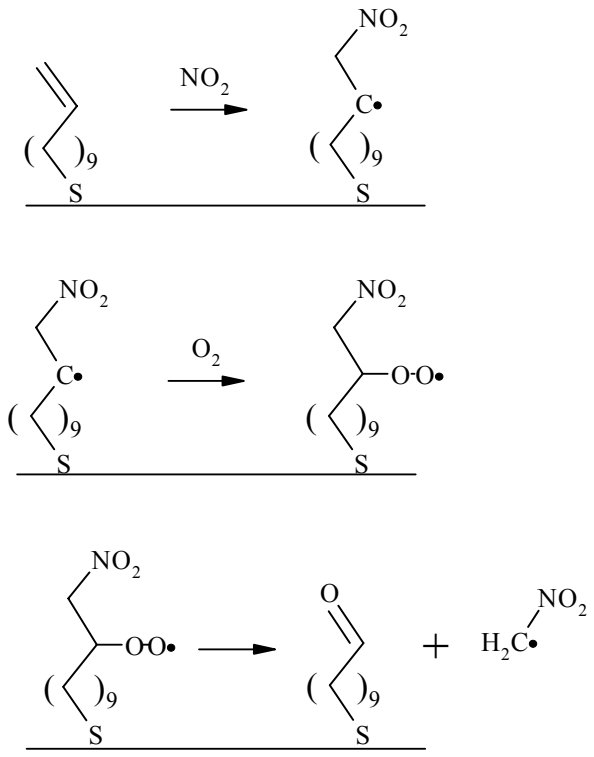

Figure 3.10: Formation of an aldehyde-terminated monolayer via the addition of NO_2 to the olefin-terminated monolayer

3.5 Summary

Exposure of an olefin-terminated self-assembled monolayer to nitrogen dioxide was preformed in order to study the gas-surface reaction. Using RAIRS and XPS, it was determined that upon exposure, an aldehyde-terminated monolayer was formed. Two mechanisms were proposed for the reaction between nitrogen dioxide and the olefin-terminated monolayer. Both result in an aldehyde-terminated SAM and follow the data present, but a determination of one over the other can not be made without further studies. First, hydrogen abstraction of the α-hydrogen by NO_2 could result in the aldehyde-terminated monolayer after further reactions with oxygen. In this mechanism, the olefin-group would be released into the gas phase as a radical. In the second proposed mechanism, NO_2 adds to the double bond proceeded by addition of oxygen. Further rearrangements could then result in the aldehyde-terminated monolayer. For the second mechanism, a gas phase by product would be formaldehyde. Further studies could include the detection of this species. The presence of oxygen is important to both of these mechanisms. Studies varying the concentration of oxygen in the system as well as the reaction in the absence of oxygen would further help to understand the interfacial reactions of gas phase nitrogen dioxide with an olefin-terminated monolayer.

References

(1) Putman, E; van Golde, L; Haagsman, H *Lung* **1997**, *175*, 75.
(2) van der Vliet, A *et al. FEBS Letters* **1994**, *339*, 89.
(3) Beckman, J *et al. Proc. Natl. Acad. Sci. USA* **1990**, *87*, 1620.
(4) Jacob, D J *Atmospheric Environment* **2000**, *34*, 2131.
(5) Tobias, H J; Ziemann, P J *Journal of Physical Chemistry A* **2001**, *105*, 6129.
(6) Feltham, E J *et al. Spectrochimica Acta Part A* **2000**, *56*, 2605.
(7) Hoffmann, T *et al. Journal of Atmospheric Chemistry* **1997**, *26*, 189.
(8) Lai, C C; Finlayson-Pitts, B J; Willis, W V *Chemical Research in Toxicology* **1990**, *3*, 517.
(9) Finlayson-Pitts, B J *et al. Inhalation Toxicology* **1994**, *6*, 267.
(10) Crapo, J *et al. American Revies of Respiratory Diseases* **1992**, *145*, 1506.
(11) Muller, B *et al. Lung* **1994**, *172*, 61.
(12) Crim, C; Longmore, W *American Journal of Physiology* **1995**, *268*, L129.
(13) Rice, K *et al. American Journal of Physiology* **1992**, *263*, L430.
(14) Nachtman, J P *et al. Journal of Toxicology and Environmental Health* **1986**, *19*, 127.
(15) Haddad, I *et al. American Journal of Physiology* **1993**, *265*, L555.
(16) Huber, G L *et al. Archives of Internal Medicine* **1971**, *128*, 81.
(17) Pryor, W A; Squadrito, G L; Friedman, M *Free Radical Biology and Medicine* **1995**, *19*, 935.
(18) Pryor, W A; Squadrito, G L; Friedman, M *Toxicology Letters* **1995**, *82/83*, 287.
(19) Wadia, Y *et al. Langmuir* **2000**, *16*, 9321.
(20) Pryor, W A; Lightsey, J W *Science* **1981**, *214*, 435.
(21) Lai, C C; Finlayson-Pitts, B J *Lipids* **1991**, *26*, 306.
(22) Niki, H *et al. International Journal of Chemical Kinetics* **1986**, *18*, 1235.
(23) Giamalva, D H *et al. Journal American Chemical Society* **1987**, *109*, 7059.
(24) Pryor, W A; Lightsey, J W; Church, D F *Journal American Chemical Society* **1982**, *104*, 6685.
(25) Kenley, R A; Hendry, D G *Journal American Chemical Society* **1982**, *104*, 220.
(26) Lachowicz, D R; Kreuz, K L *Journal Organic Chemistry* **1967**, *32*, 3885.
(27) Akimoto, H; Sprung, J L; Pitts, J J N *Journal American Chemical Society* **1972**, *94*, 4850.
(28) Atkinson, R *et al. International Journal of Chemical Kinetics* **1984**, *16*, 697.
(29) Sprung, J L; Akimoto, H; Pitts, J, J.N. *Journal American Chemical Society* **1971**, *93*, 4358.
(30) Sprung, J L; Akimoto, H; Pitts, J, J.N. *Journal American Chemical Society* **1974**, *96*, 6549.
(31) Shechter, H; Gardikes, J; Pagano, A *Journal American Chemical Society* **1959**, *81*, 5420.
(32) Khan, N A *Journal of Chemical Physics* **1955**, *23*, 2447.
(33) Ulman, A *Chemical Reviews* **1996**, *96*, 1533.
(34) Schlotter, N *et al. Chemical Physics Letters* **1986**, *132*, 93.

(35) Ogawa, H; Chihera, T; Taya, K *Journal American Chemical Society* **1985**, *107*, 1365.
(36) Allara, D; Nuzzo, R *Langmuir* **1985**, *1*, 52.
(37) Allara, D; Nuzzo, R *Langmuir* **1985**, *1*, 45.
(38) Porter, M *et al. Journal American Chemical Society* **1987**, *109*, 3559.
(39) Nuzzo, R; Dubois, L; Allara, D *Journal American Chemical Society* **1990**, *112*, 558.
(40) Laibinis, P *et al. Journal American Chemical Society* **1991**, *113*, 7152.
(41) Dubois, L; Zegarski, B; Nuzzo, R *Journal American Chemical Society* **1990**, *112*, 570.
(42) Bain, C *et al. Journal American Chemical Society* **1989**, *111*, 321.
(43) Hickman, J *et al. Journal American Chemical Society* **1991**, *113*, 1128.
(44) Nuzzo, R; Zegarski, B; Dubois, L *Journal American Chemical Society* **1987**, *109*, 733.
(45) Schlenoff, J; Li, M; Ly, H *Journal American Chemical Society* **1995**, *117*, 12528.
(46) Delamarche, E *et al. Langmuir* **1994**, *10*, 4103.
(47) Poirier, G; Pylant, E; White, J *Journal of Chemical Physics* **1996**, *104*, 7325.
(48) Poirier, G; Tarlov, M *Langmuir* **1994**, *10*, 2853.
(49) Touzov, I; Gorman, C *Journal of Physical Chemistry B* **1997**, *101*, 5263.
(50) Jensen-Gronbech, N *et al. Langmuir* **2003**, *19*, 1474.
(51) Camillone, N *et al. Journal of Chemical Physics* **1993**, *98*, 35033511.
(52) Chidsey, C; Loiacono, D *Langmuir* **1990**, *6*, 682.
(53) Dubois, L; Zegarski, B; Nuzzo, R *Journal of Chemical Physics* **1993**, *98*, 678.
(54) Kato, H S *et al. Journal of Physical Chemistry B* **2002**, *106*, 9655.
(55) Peanasky, J S; McCarley, R L *Langmuir* **1998**, *14*, 113.
(56) Leung, T; Structure and Growth of Modified Thiol Monolayers on Au(111), *PhD Thesis*, Princeton University; 1998.
(57) Fenter, P; Eberhardt, A; Eisenberger, P *Science* **1994**, *226*, 1216.
(58) Fenter, P *et al. Surface Science* **1998**, *412/413*, 213.
(59) Kluth, G; Carraro, C; Maboudian, R *Physical Review B* **1999**, *59*, R10449.
(60) Zerulla, D; Chasse, T *Langmuir* **1999**, *15*, 5285.
(61) Fischer, D; Curioni, A; Andreoni, W *Langmuir* **2003**, *19*, 3567.
(62) Sullivan, T P; Huck, W T S *Europe Journal of Organic Chemistry* **2003**, 17.
(63) Clark, J; Macquarrie, D *Chemical Society Reviews* **1996**, *25*, 303.
(64) Ricco, A; Crooks, R; Osbourn, G *Accounts of Chemical Research* **1998**, *31*, 289.
(65) Everhart, D *Chemtech* **1999**, *29*, 30.
(66) Mirkin, C; Ratner, M *Annual Review of Physical Chemistry* **1992**, *43*, 719.
(67) Chechik, V; Crooks, R; Stirling, C J M *Advanced Materials* **2000**, *12*, 1161.
(68) Mrksich, M; Whitesides, G M *Annual Review of Biophysics and Biomolecular Structure* **1996**, *25*, 55.
(69) Mrksich, M *Current Opinion in Chemical Biology* **2002**, *6*, 794.
(70) Su, J; Mrksich, M *Langmuir* **2003**, *19*, 4867.
(71) Fryxell, G *et al. Langmuir* **1996**, *12*, 5064.
(72) Kwon, Y; Mrksich, M *Journal American Chemical Society* **2002**, *124*, 806.
(73) Dordi, B; Schonherr, H; Vancso, G J *Langmuir* **2003**, *19*, 5780.
(74) Fukuda, K *et al. Advanced in Colloid and Interface Science* **2000**, *87*, 113.
(75) Bartz, M *et al. Angewandte Chemie, International Edition* **1998**, *37*, 2466.

(76) Lui, M *et al. Chemistry Letters* **1993**, *6*, 967.
(77) Tollner, K *et al. Science* **1997**, *278*, 2100.
(78) Schonherr, H *et al. Journal American Chemical Society* **2000**, *122*, 3679.
(79) Vericat, C *et al. Journal of Physical Chemistry B* **2002**, *106*, 9114.
(80) Kraft, M; Moore, J *Langmuir* **2003**, *19*, 910.
(81) Wasserman, S R; Tao, Y; Whitesides, G M *Langmuir* **1989**, *5*, 1074.
(82) Maoz, R; Sagiv, J *Langmuir* **1987**, *3*, 1045.
(83) Maoz, R; Sagiv, J *Langmuir* **1987**, *3*, 1034.
(84) Maoz, R; Sagiv, J *Thin Solid Films* **1985**, *132*, 135.
(85) Lai, C C; Yang, S; Finlayson-Pitts, B J *Langmuir* **1994**, *10*, 4637.
(86) Finlayson-Pitts, B J; Sweetman, L L; Weissbart, B *Toxicology and Applied Pharmacology* **1987**, *89*, 438.
(87) Criegee, R *Angewandte Chemie* **1975**, *87*, 765.
(88) Patai, S, Ed. *Chemistry of the Thiol Group*; Wiley: New York, 1974.
(89) Czanderna, A, Ed. *Methods of Surface Analysis*; Elsevier Science: New York, 1989.
(90) Allerhand, A; Schleyer, P *Journal American Chemical Society* **1963**, *85*, 1715.
(91) Hobza, P; Havlas, Z *Chemical Reviews* **2000**, *100*, 4253.
(92) Alabugin, I *et al. Journal American Chemical Society* **2003**, *125*, 5973.
(93) Nuzzo, R; Fusco, F; Allara, D *Journal American Chemical Society* **1987**, *109*, 2358.
(94) Horton, R; Herne, T; Myles, D *Journal American Chemical Society* **1997**, *119*, 12980.
(95) Kim, T K *et al. Journal of Physical Chemistry B* **2000**, *104*, 7403.
(96) Weiner, B R; Barnhard, K I In *N-Centered Radicals*; Alfassi, Z B, Ed.; Wiley & Sons: New York, 1998, pp 39.

Appendix

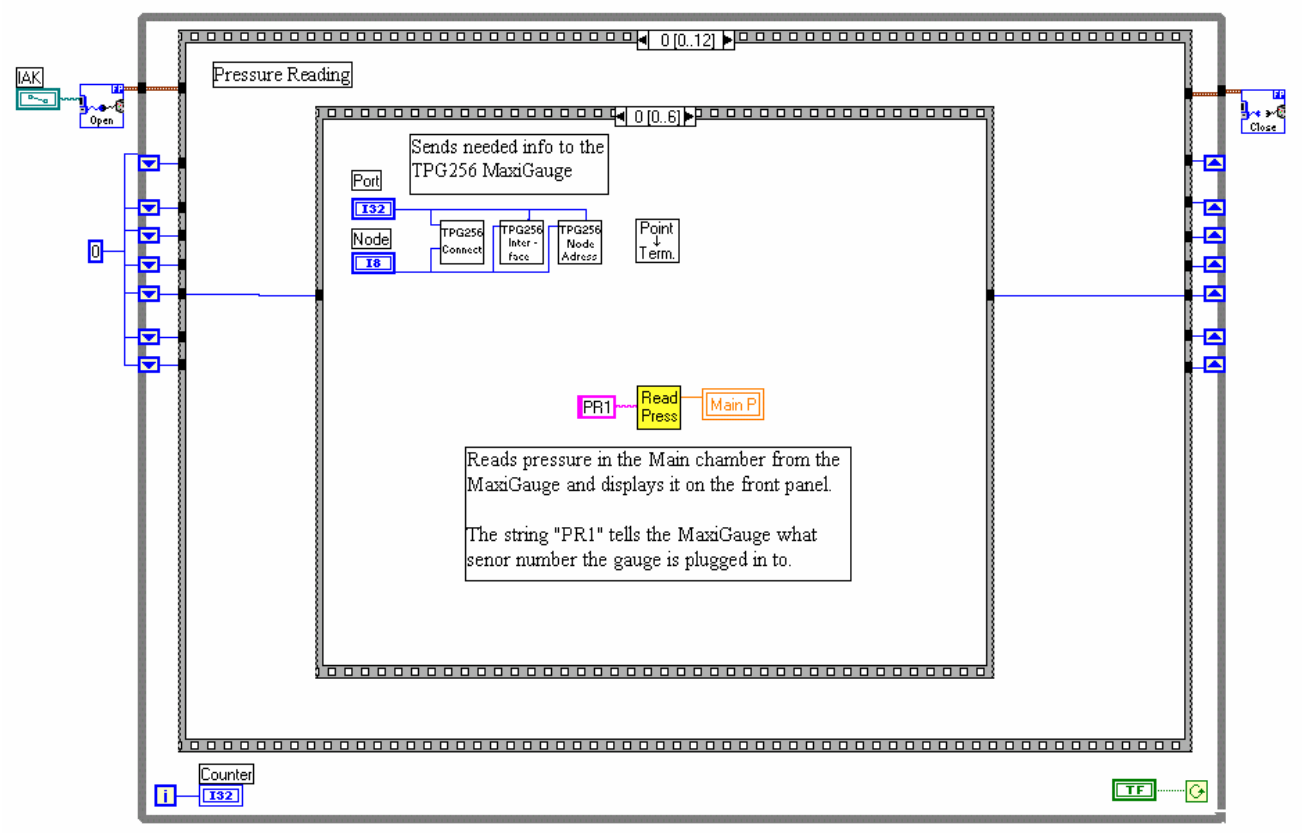

Figure A.1: Pressures are read from the main gauge controller

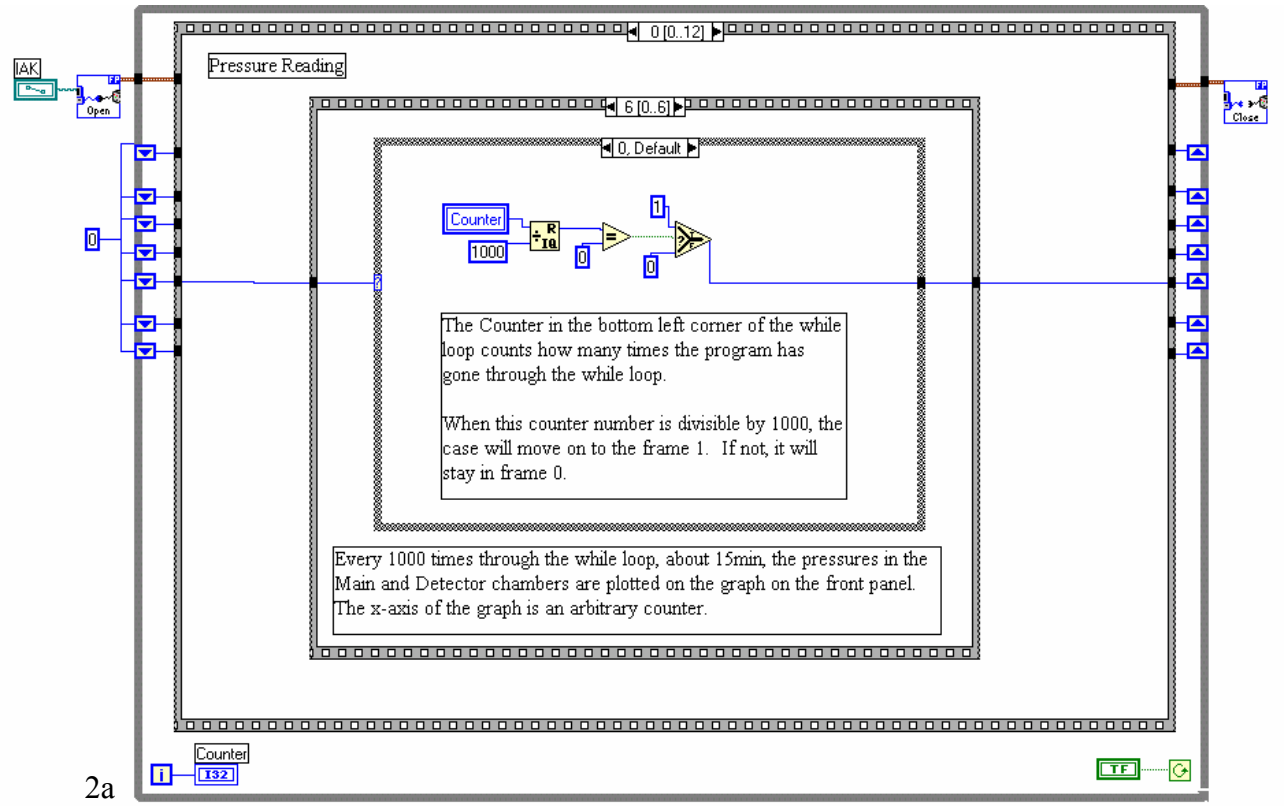

2a

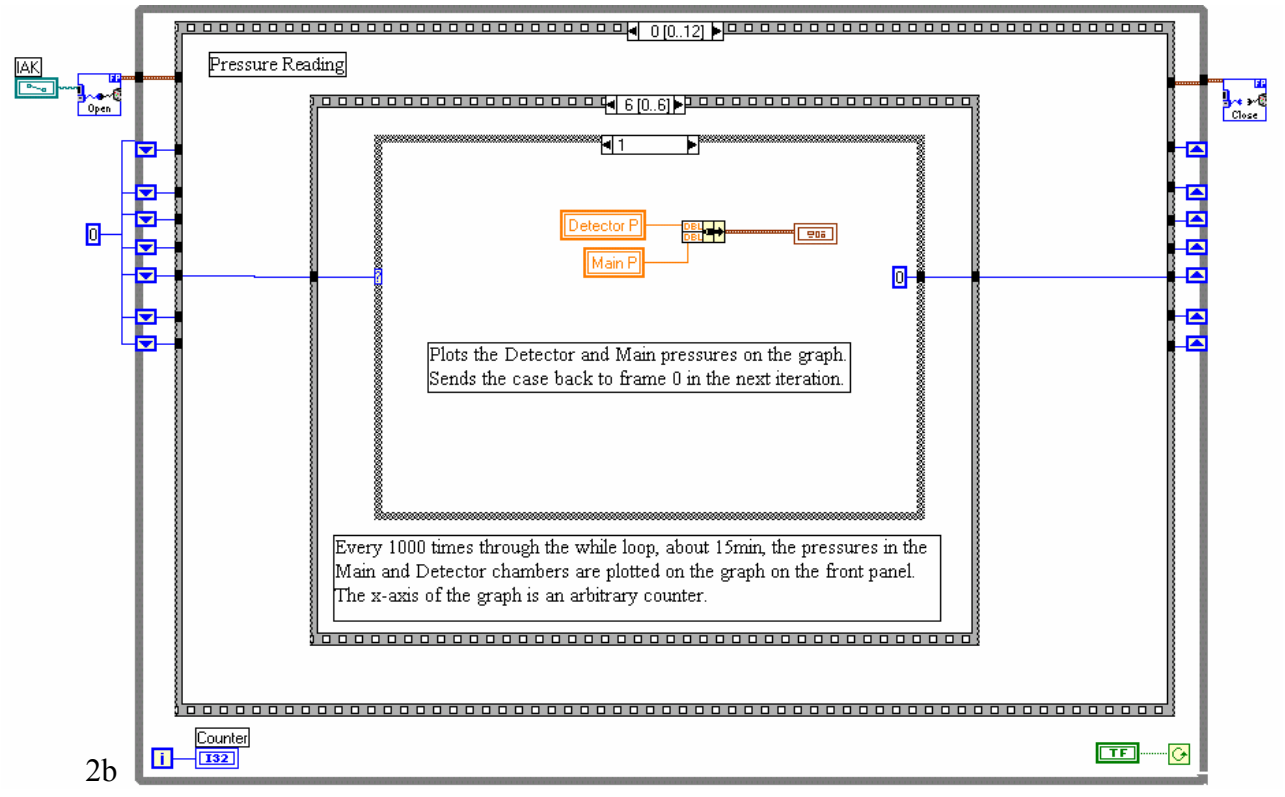

2b

Figure A.2: Main and detector chamber pressures are plotted on the front panel

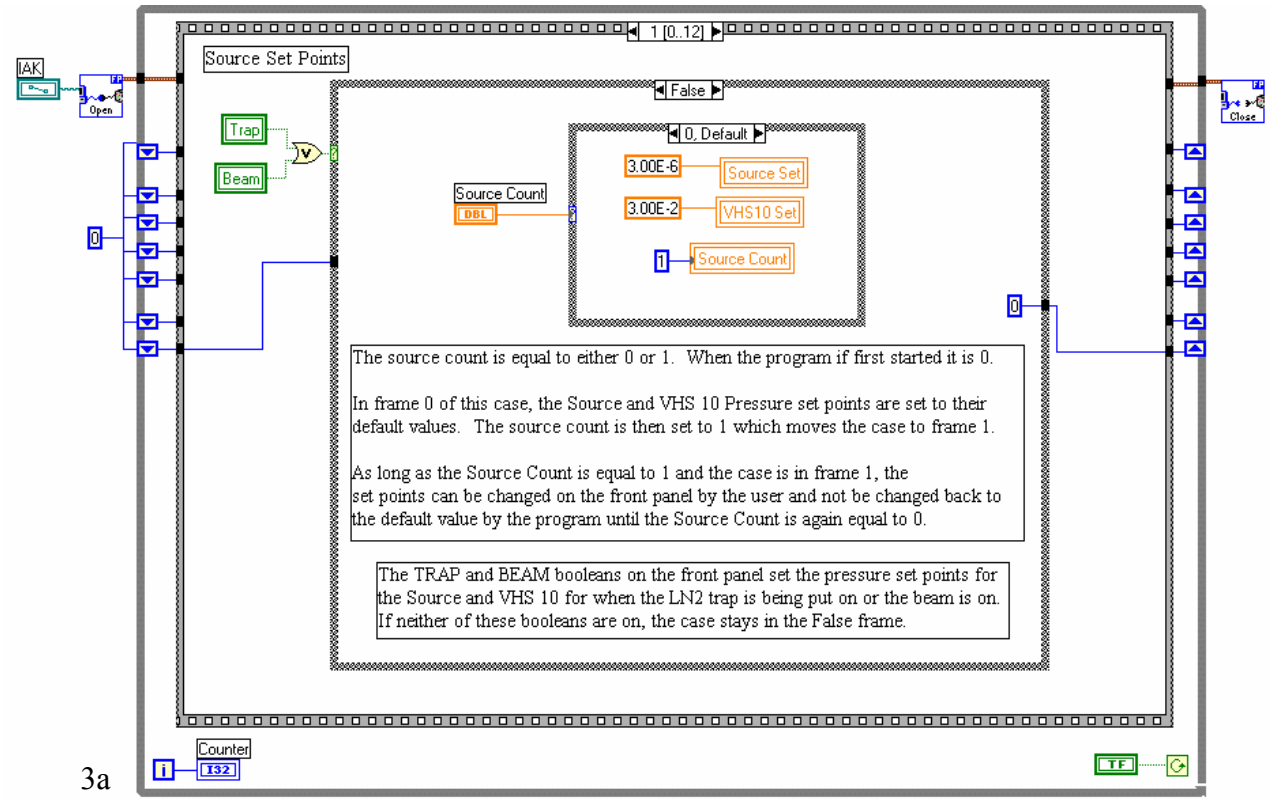
1 [0..12]
Source Set Points
False
Trap
Beam
0
0, Default
3.00E-6
Source Set
3.00E-2
VHS10 Set
Source Count
DBL
1
Source Count
0
The source count is equal to either 0 or 1. When the program if first started it is 0.
In frame 0 of this case, the Source and VHS 10 Pressure set points are set to their default values. The source count is then set to 1 which moves the case to frame 1.
As long as the Source Count is equal to 1 and the case is in frame 1, the set points can be changed on the front panel by the user and not be changed back to the default value by the program until the Source Count is again equal to 0.
The TRAP and BEAM booleans on the front panel set the pressure set points for the Source and VHS 10 for when the LN2 trap is being put on or the beam is on. If neither of these booleans are on, the case stays in the False frame.
IAK
Open
Close
Counter
I32
TF

3a

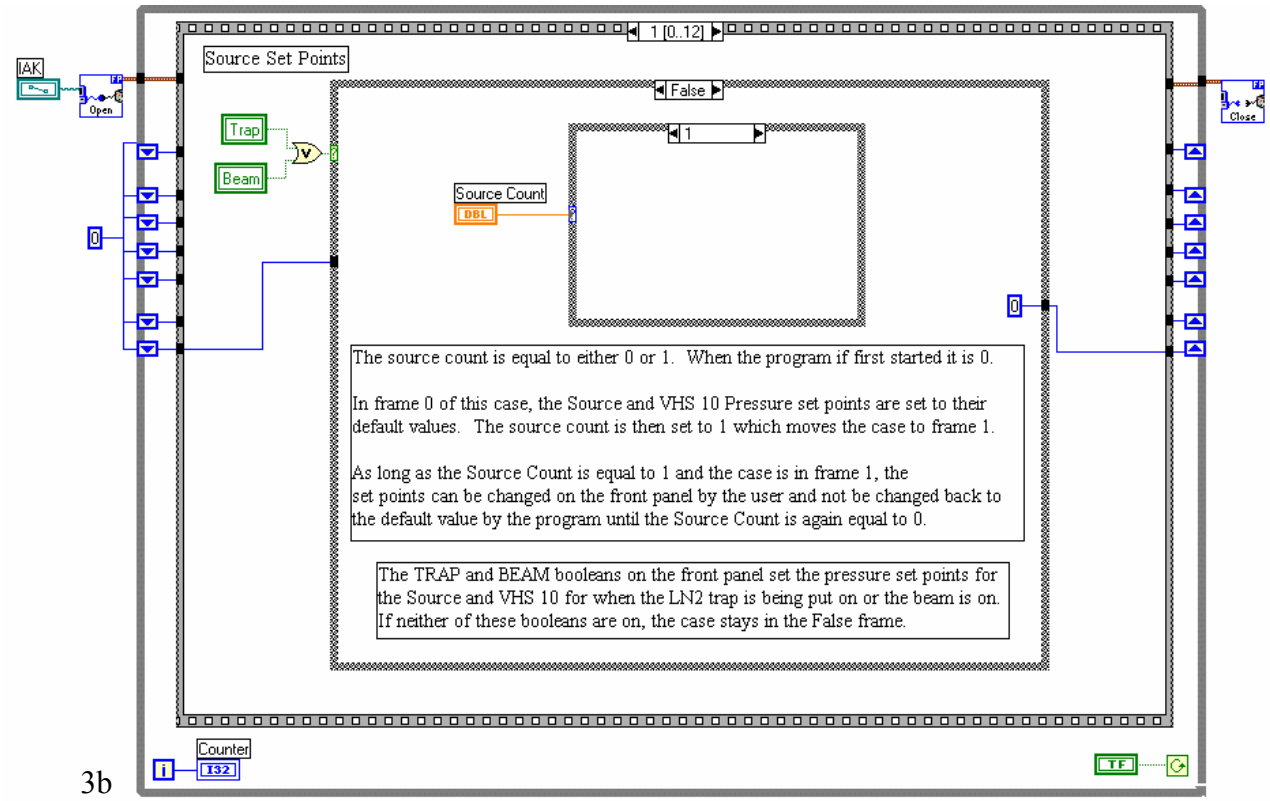
1 [0..12]
Source Set Points
False
Trap
Beam
0
1
Source Count
DBL
0
The source count is equal to either 0 or 1. When the program if first started it is 0.
In frame 0 of this case, the Source and VHS 10 Pressure set points are set to their default values. The source count is then set to 1 which moves the case to frame 1.
As long as the Source Count is equal to 1 and the case is in frame 1, the set points can be changed on the front panel by the user and not be changed back to the default value by the program until the Source Count is again equal to 0.
The TRAP and BEAM booleans on the front panel set the pressure set points for the Source and VHS 10 for when the LN2 trap is being put on or the beam is on. If neither of these booleans are on, the case stays in the False frame.
IAK
Open
Close
Counter
I32
TF

3b

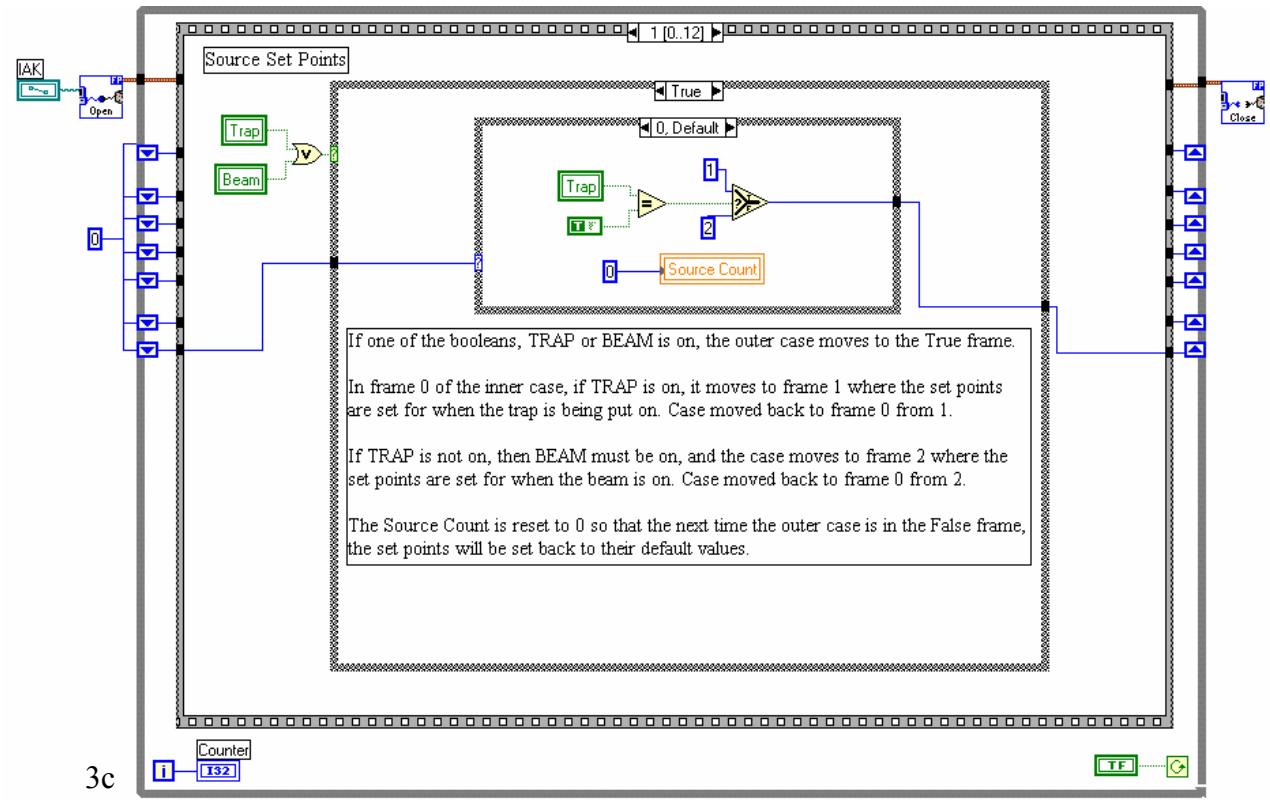
IAK
Open
1 [0..12]
Source Set Points
True
0, Default
Trap
Beam
Source Count
Close
If one of the booleans, TRAP or BEAM is on, the outer case moves to the True frame.
In frame 0 of the inner case, if TRAP is on, it moves to frame 1 where the set points are set for when the trap is being put on. Case moved back to frame 0 from 1.
If TRAP is not on, then BEAM must be on, and the case moves to frame 2 where the set points are set for when the beam is on. Case moved back to frame 0 from 2.
The Source Count is reset to 0 so that the next time the outer case is in the False frame, the set points will be set back to their default values.
Counter
I32
TF

3c

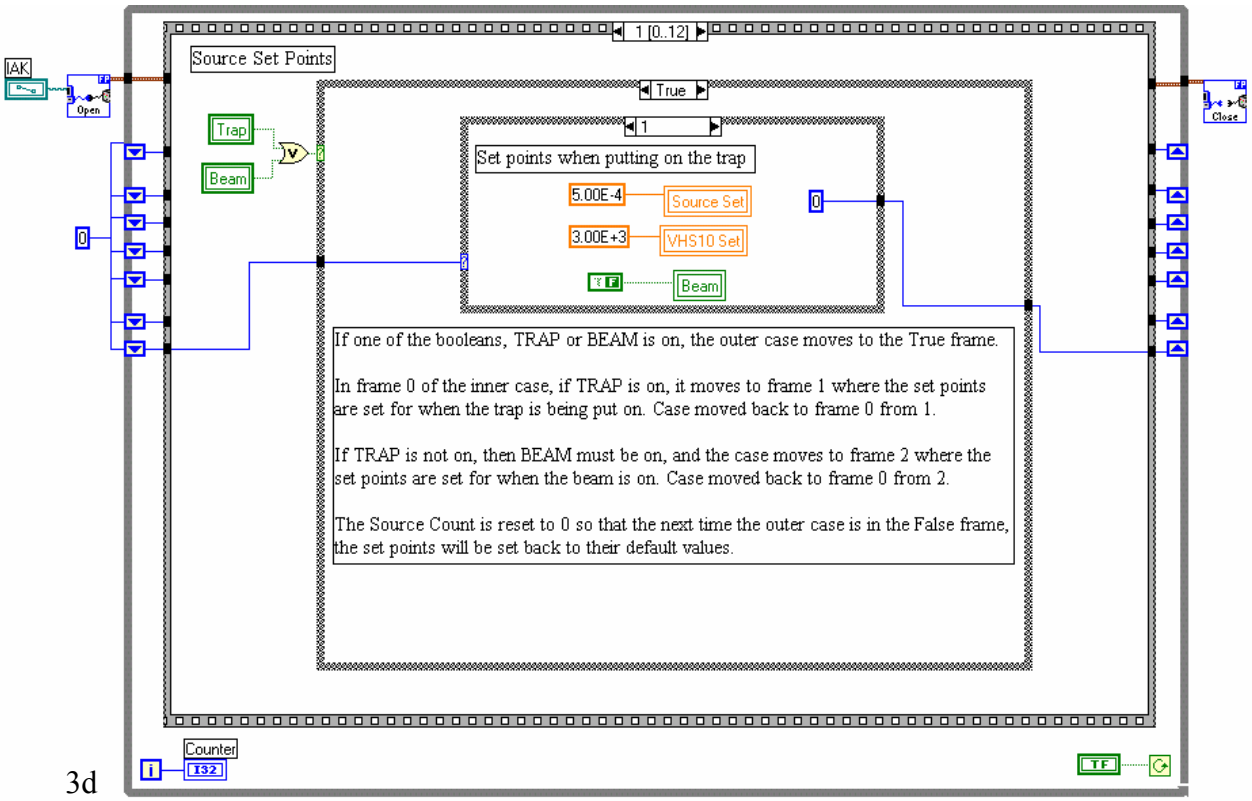
IAK
Open
1 [0..12]
Source Set Points
True
1
Set points when putting on the trap
5.00E-4
Source Set
3.00E+3
VHS10 Set
Beam
Close
If one of the booleans, TRAP or BEAM is on, the outer case moves to the True frame.
In frame 0 of the inner case, if TRAP is on, it moves to frame 1 where the set points are set for when the trap is being put on. Case moved back to frame 0 from 1.
If TRAP is not on, then BEAM must be on, and the case moves to frame 2 where the set points are set for when the beam is on. Case moved back to frame 0 from 2.
The Source Count is reset to 0 so that the next time the outer case is in the False frame, the set points will be set back to their default values.
Counter
I32
TF

3d

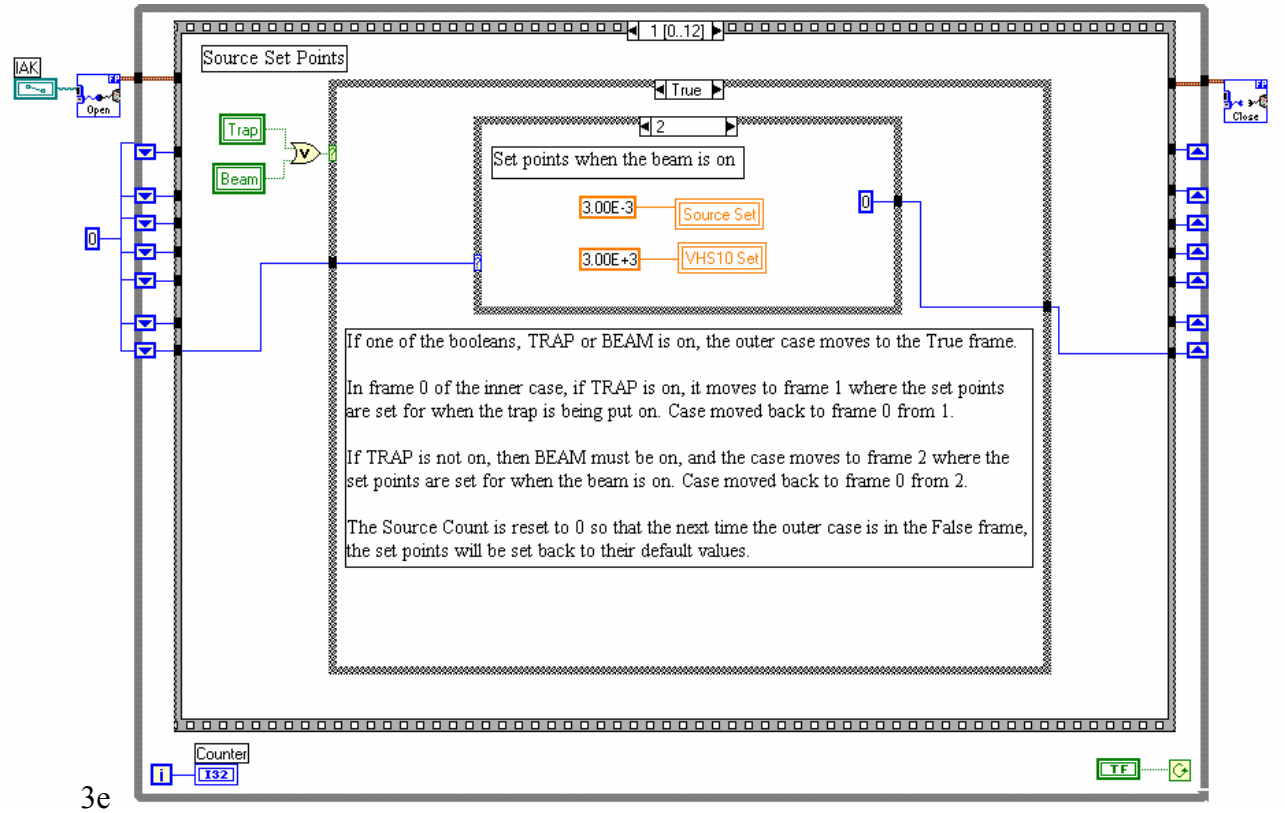

3e

Figure A.3: Source set points determined by the “Trap” and “Beam” Booleans

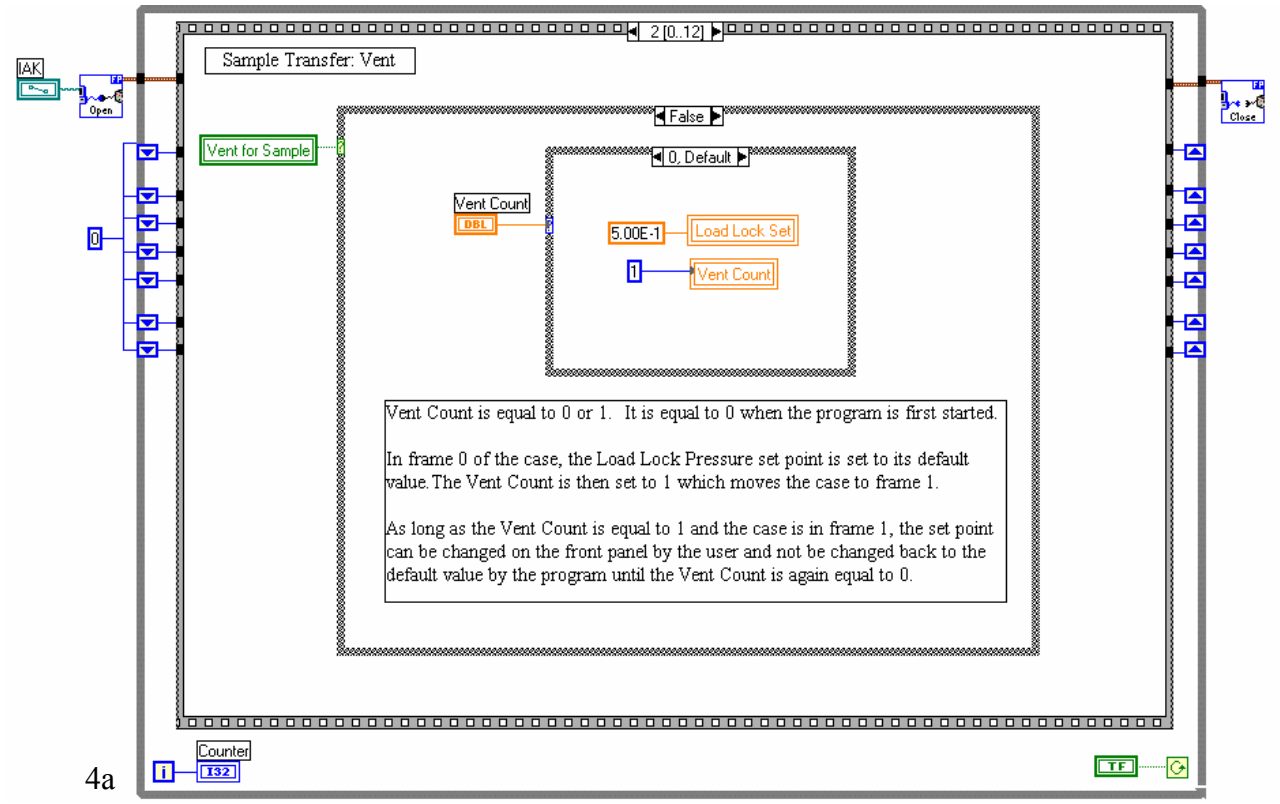
IAK
Open
2 [0..12]
Sample Transfer: Vent
False
Vent for Sample
0, Default
Vent Count
DBL
5.00E-1
Load Lock Set
1
Vent Count
Close
0
Vent Count is equal to 0 or 1. It is equal to 0 when the program is first started.
In frame 0 of the case, the Load Lock Pressure set point is set to its default value. The Vent Count is then set to 1 which moves the case to frame 1.
As long as the Vent Count is equal to 1 and the case is in frame 1, the set point can be changed on the front panel by the user and not be changed back to the default value by the program until the Vent Count is again equal to 0.
Counter
I32
TF

4a

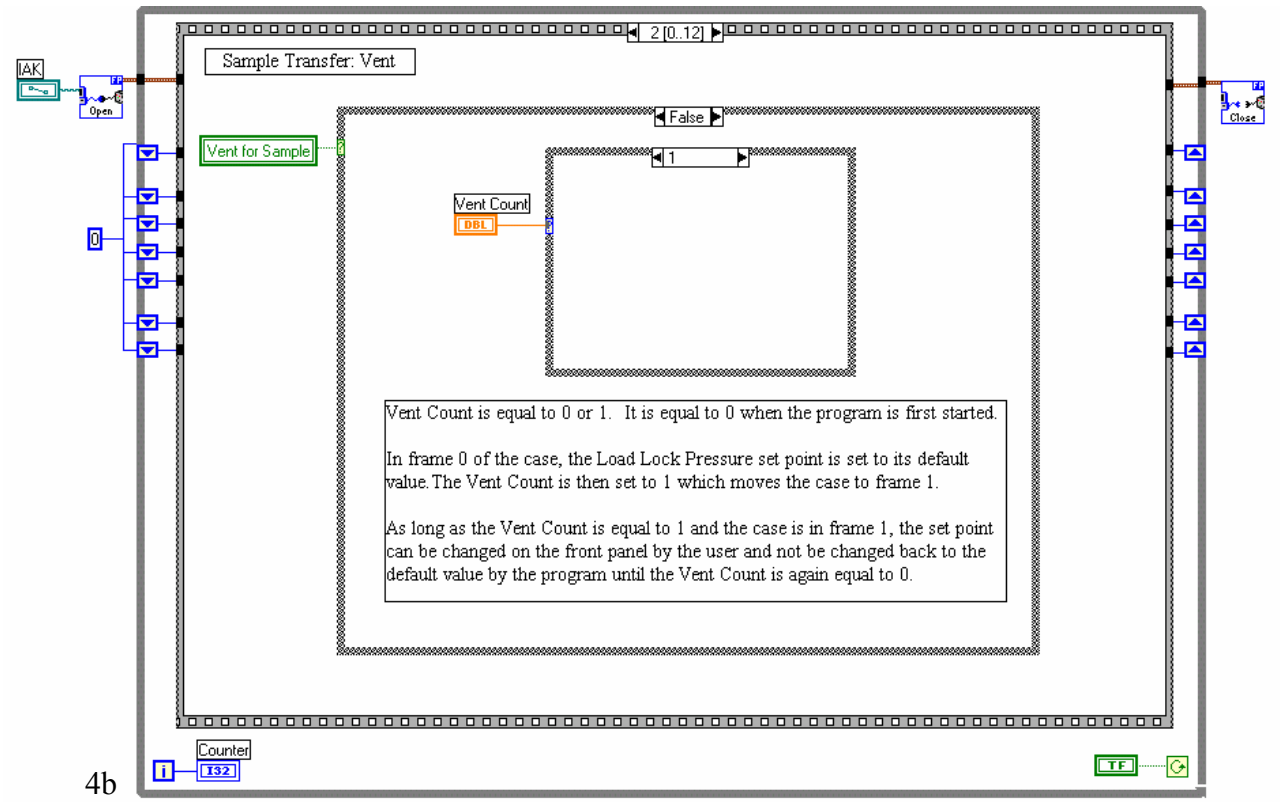
IAK
Open
2 [0..12]
Sample Transfer: Vent
False
Vent for Sample
1
Vent Count
DBL
Close
0
Vent Count is equal to 0 or 1. It is equal to 0 when the program is first started.
In frame 0 of the case, the Load Lock Pressure set point is set to its default value. The Vent Count is then set to 1 which moves the case to frame 1.
As long as the Vent Count is equal to 1 and the case is in frame 1, the set point can be changed on the front panel by the user and not be changed back to the default value by the program until the Vent Count is again equal to 0.
Counter
I32
TF

4b

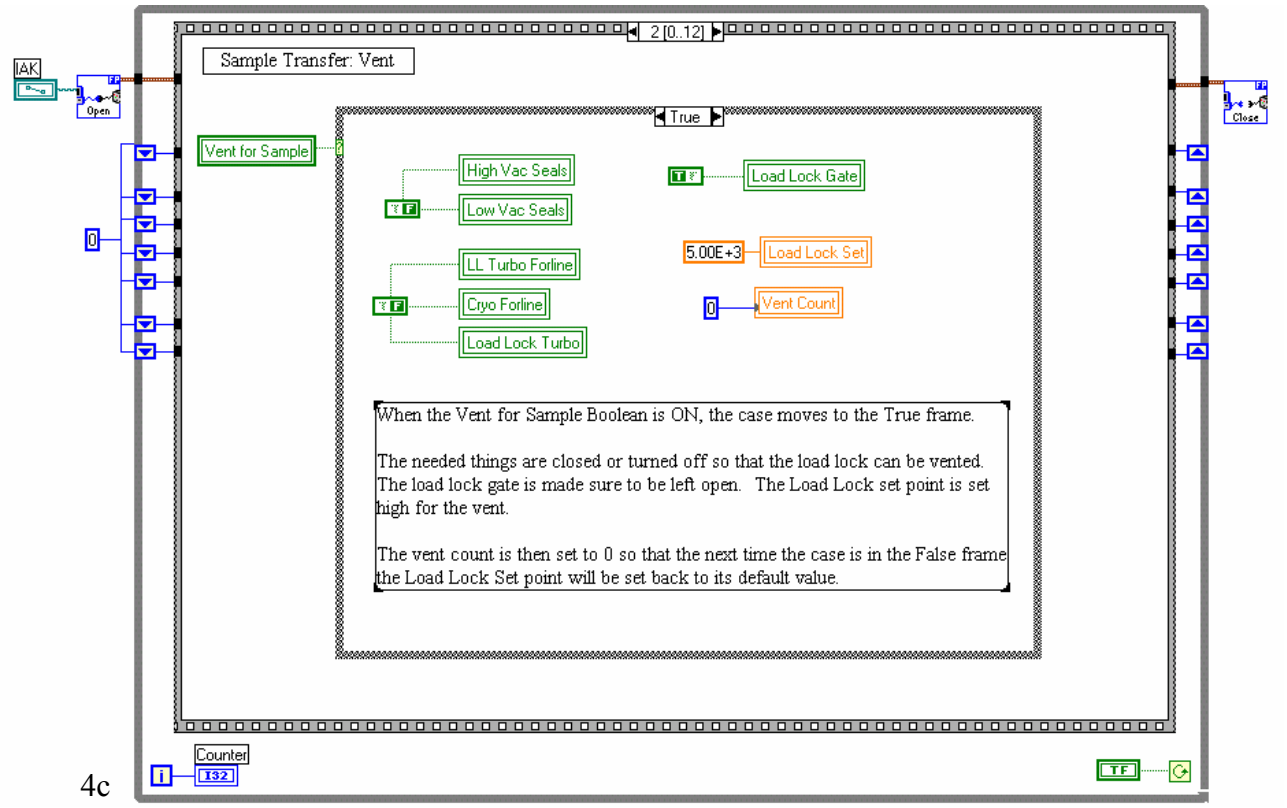

Figure A.4: "Vent for Sample" prepares the Load Lock chamber for sample introduction

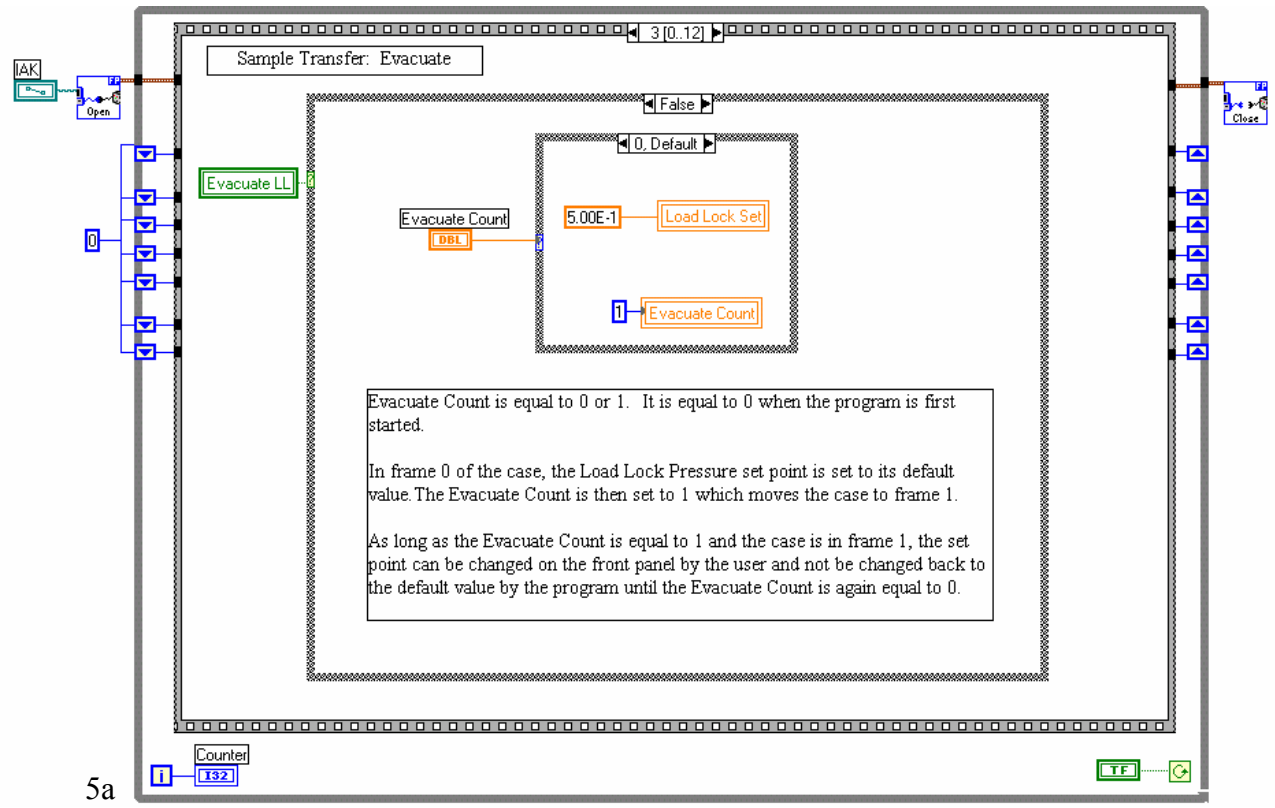
IAK
Open
3 [0..12]
Sample Transfer: Evacuate
False
0, Default
Evacuate LL
Evacuate Count
DBL
5.00E-1
Load Lock Set
1
Evacuate Count
0
Close
Evacuate Count is equal to 0 or 1. It is equal to 0 when the program is first started.
In frame 0 of the case, the Load Lock Pressure set point is set to its default value. The Evacuate Count is then set to 1 which moves the case to frame 1.
As long as the Evacuate Count is equal to 1 and the case is in frame 1, the set point can be changed on the front panel by the user and not be changed back to the default value by the program until the Evacuate Count is again equal to 0.
Counter
I32
TF

5a

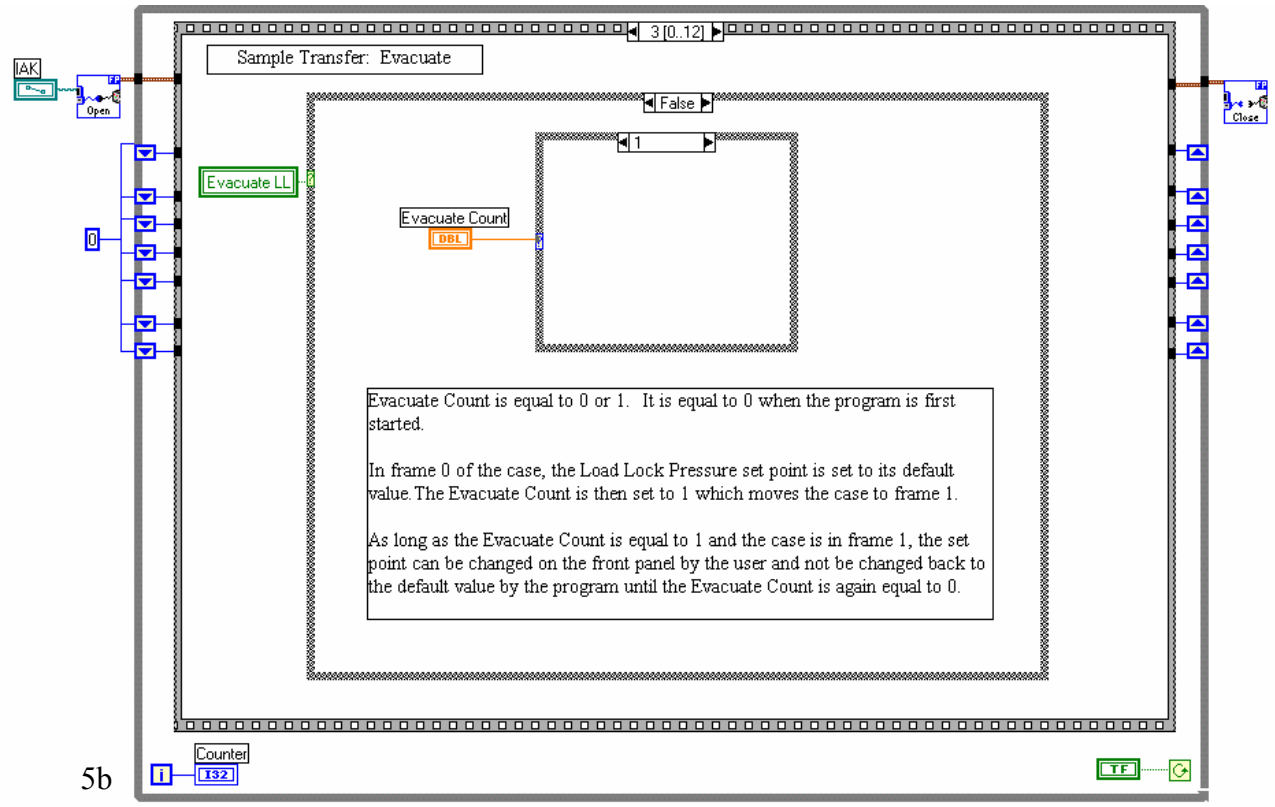
IAK
Open
3 [0..12]
Sample Transfer: Evacuate
False
1
Evacuate LL
Evacuate Count
DBL
0
Close
Evacuate Count is equal to 0 or 1. It is equal to 0 when the program is first started.
In frame 0 of the case, the Load Lock Pressure set point is set to its default value. The Evacuate Count is then set to 1 which moves the case to frame 1.
As long as the Evacuate Count is equal to 1 and the case is in frame 1, the set point can be changed on the front panel by the user and not be changed back to the default value by the program until the Evacuate Count is again equal to 0.
Counter
I32
TF

5b

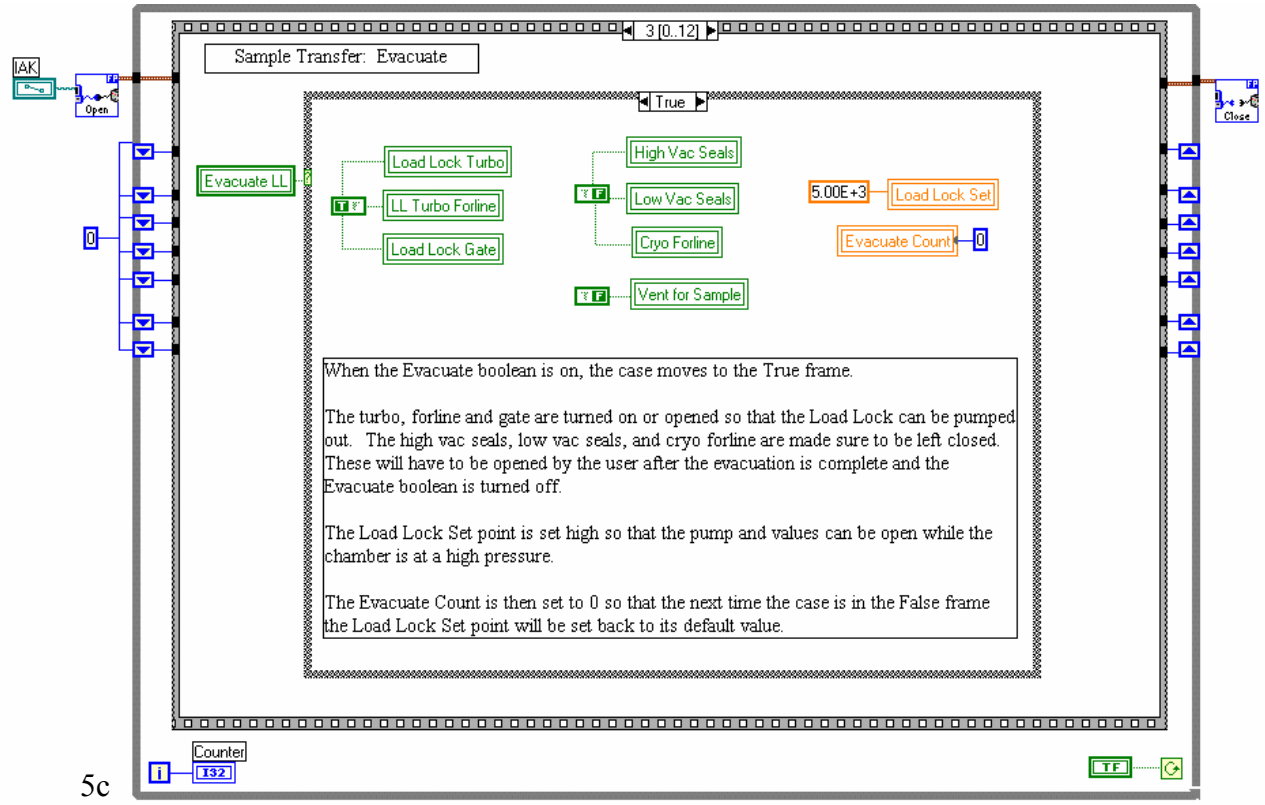

Figure A.5: "Evacuate" Boolean evacuates Load Lock chamber for sample introduction

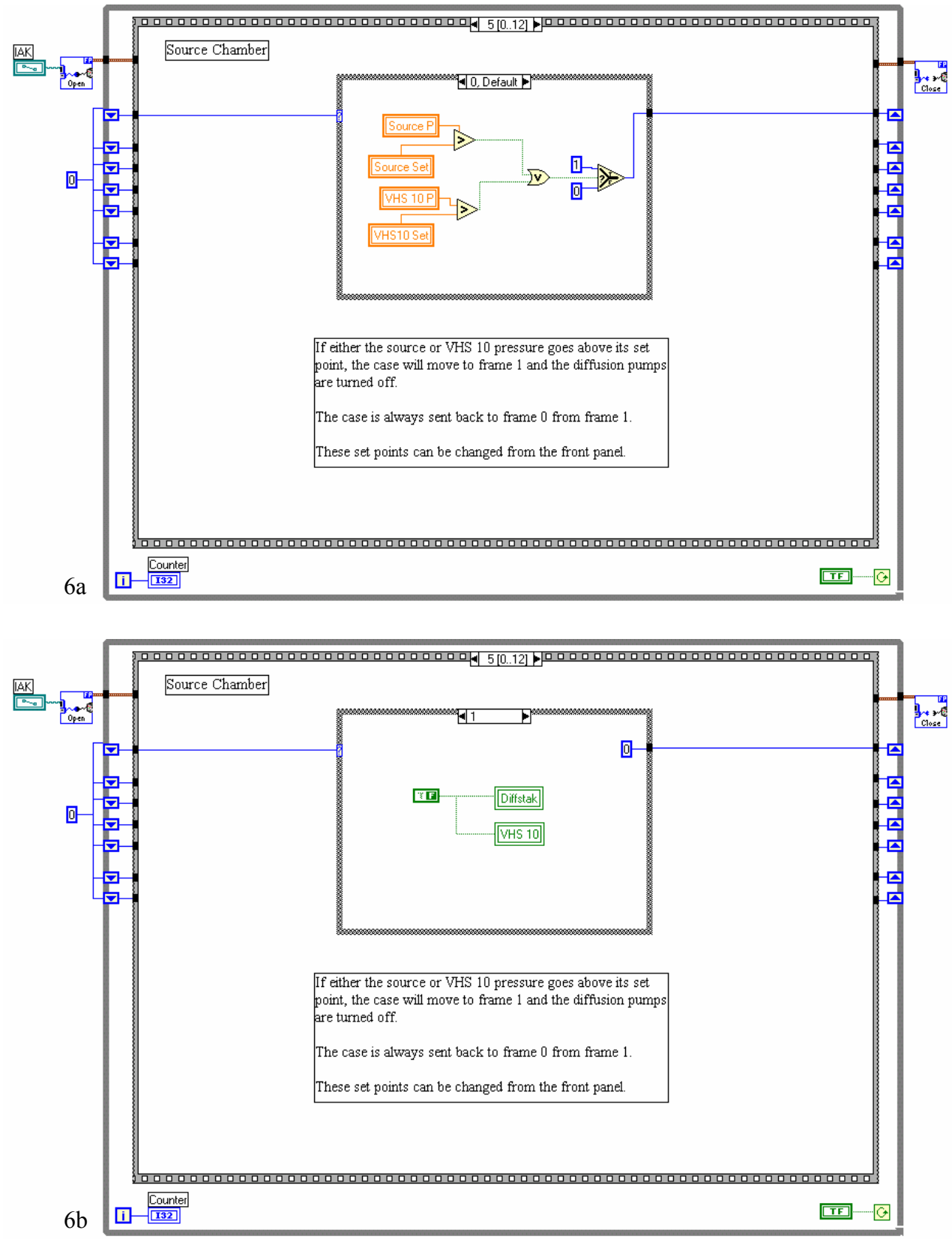

Figure A.6: Source Chamber procedures in the event of a pressure burst

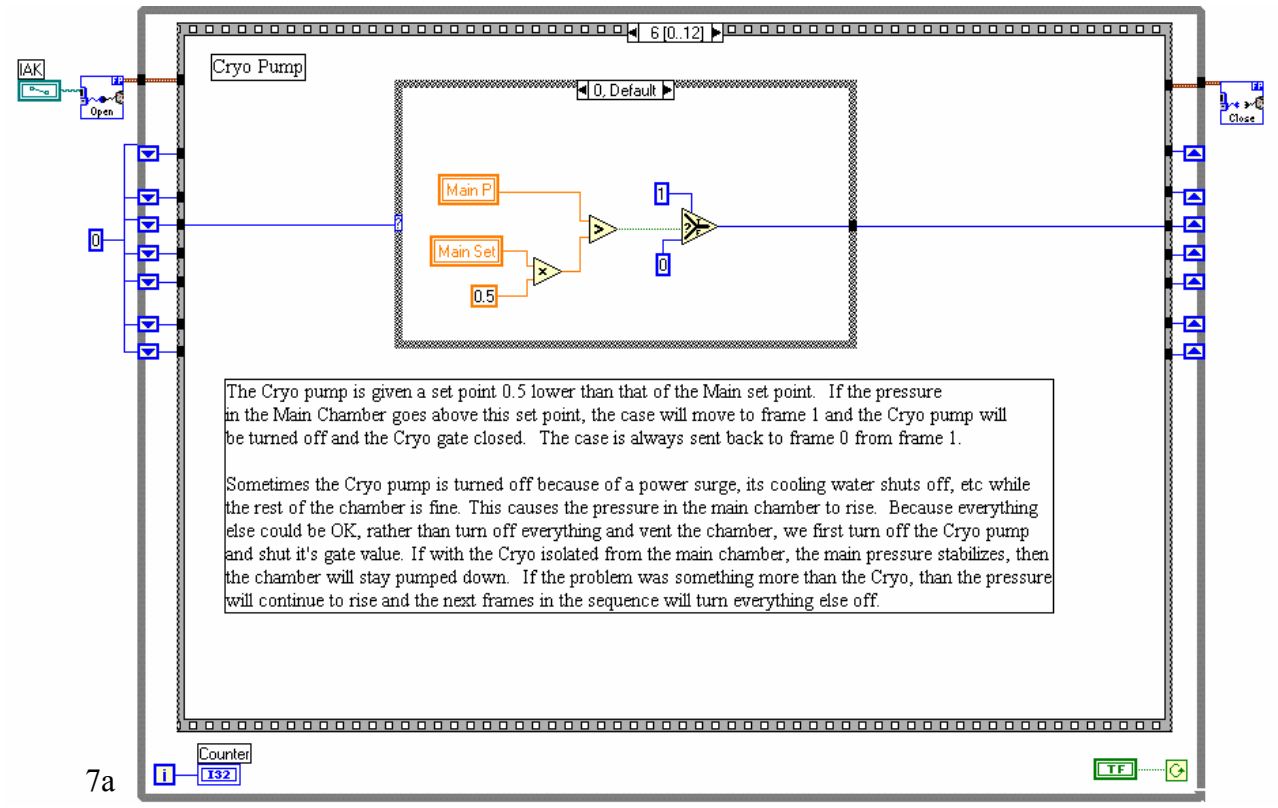

7a

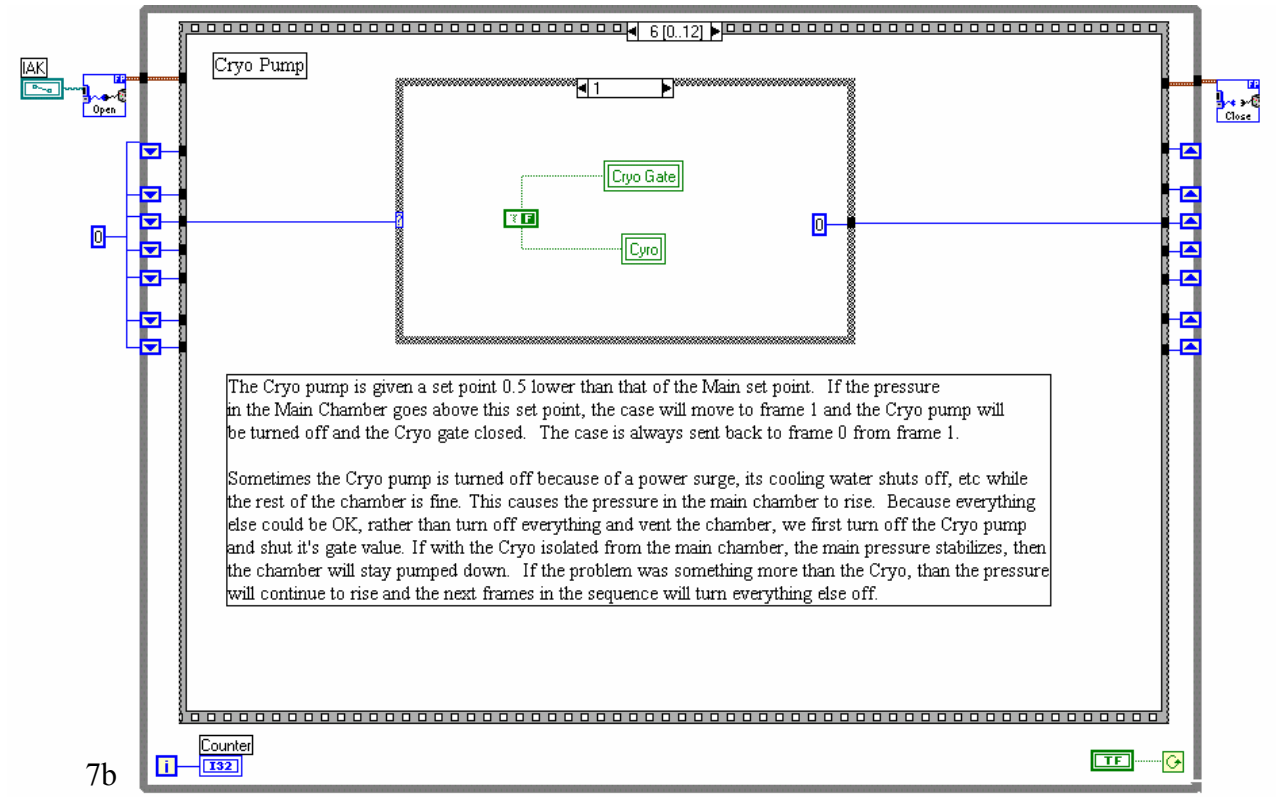

7b

Figure A.7: Cryo Pump set point

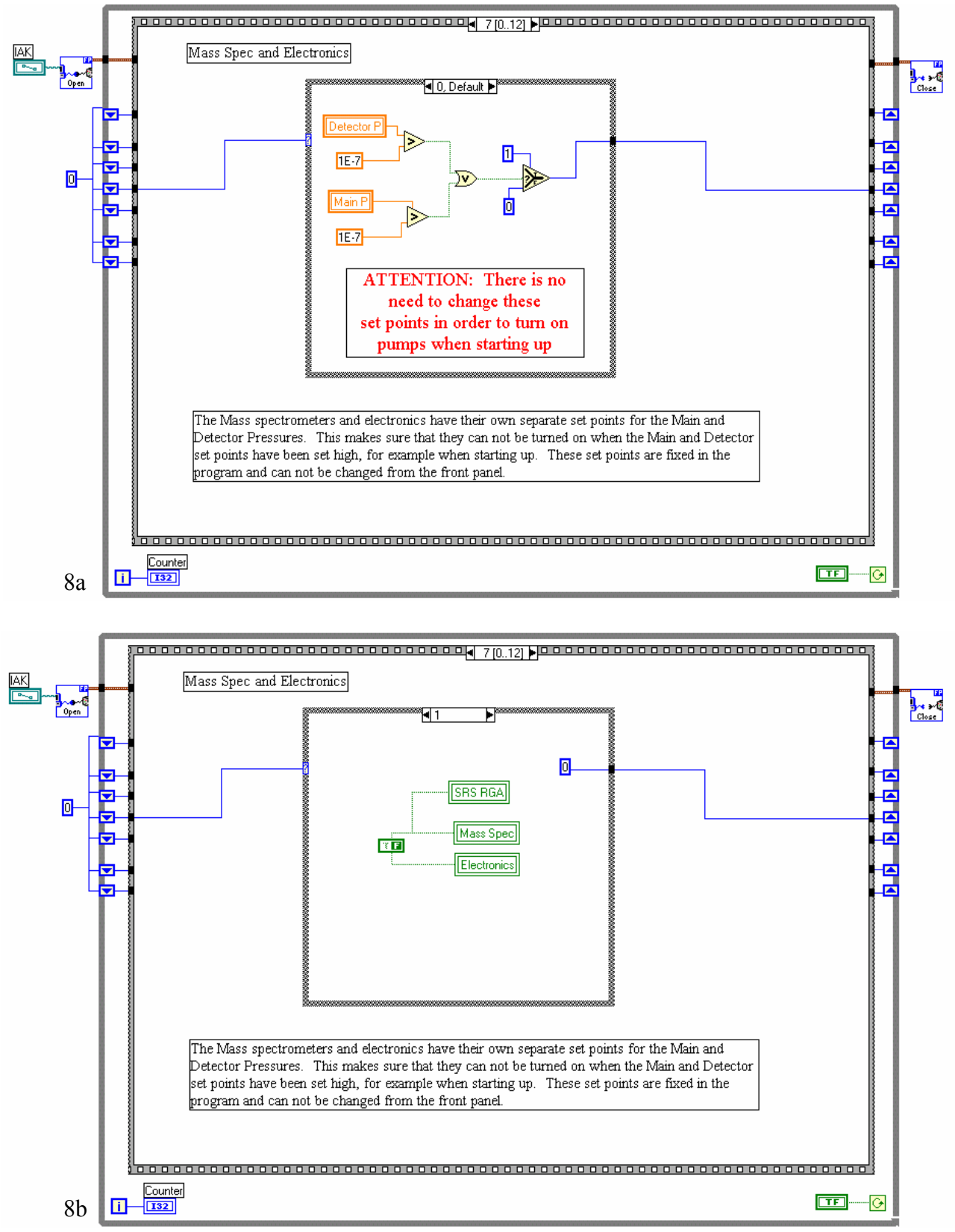

Figure A.8: Set points for the mass spectrometers and electronics

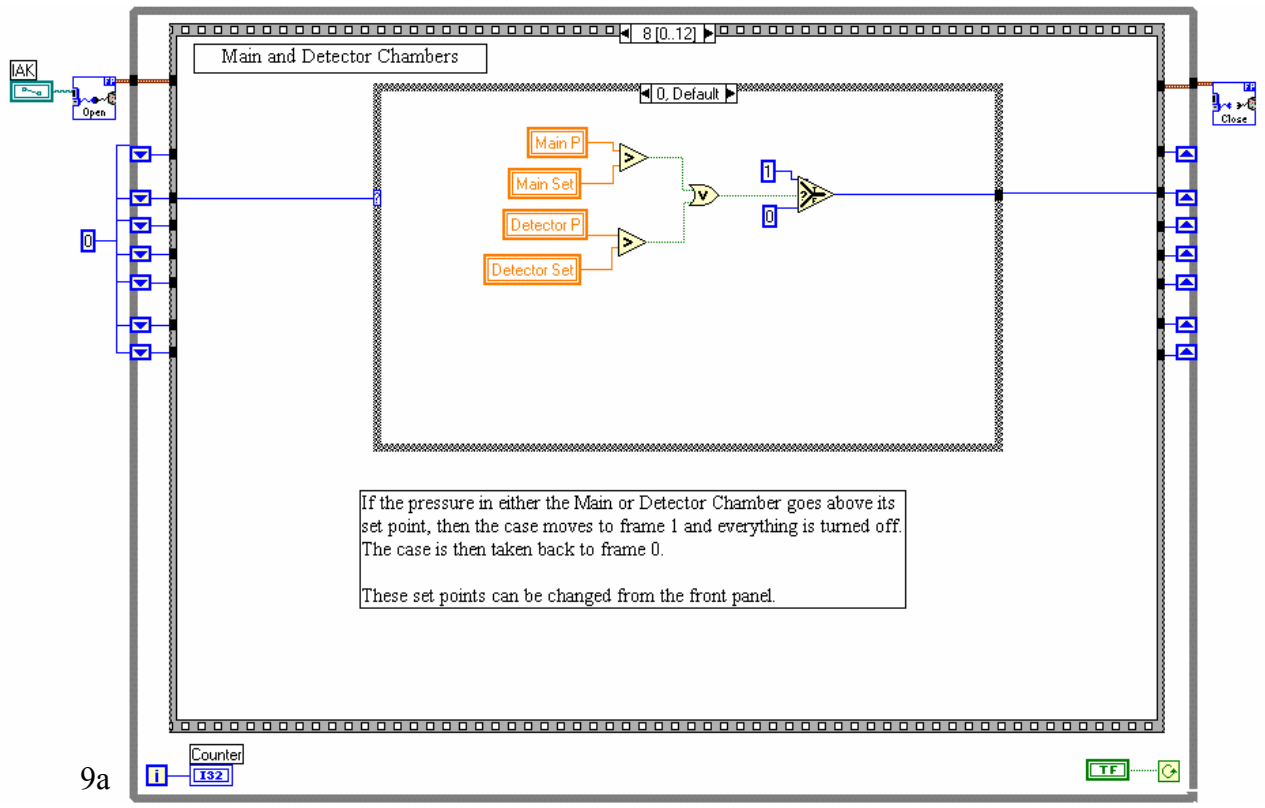

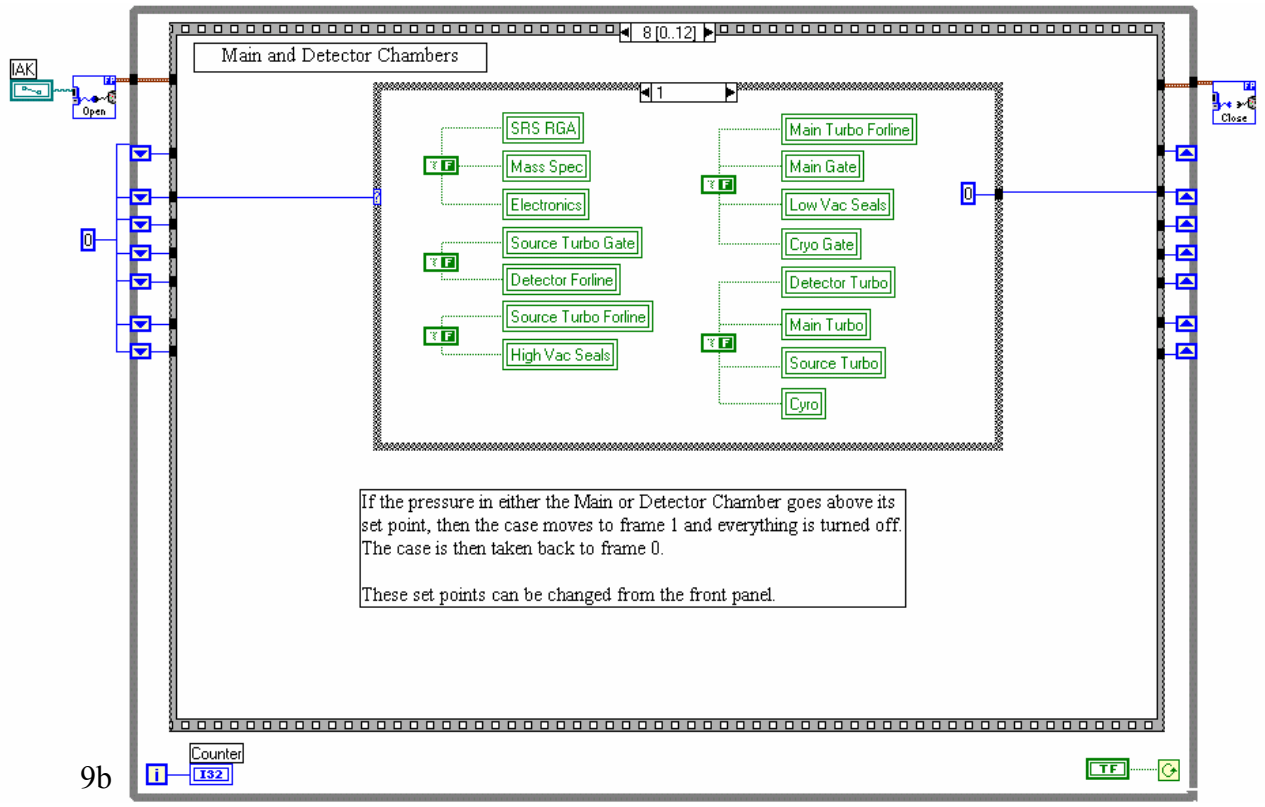

Figure A.9: Procedure for the main and detector chambers in the event of a pressure burst

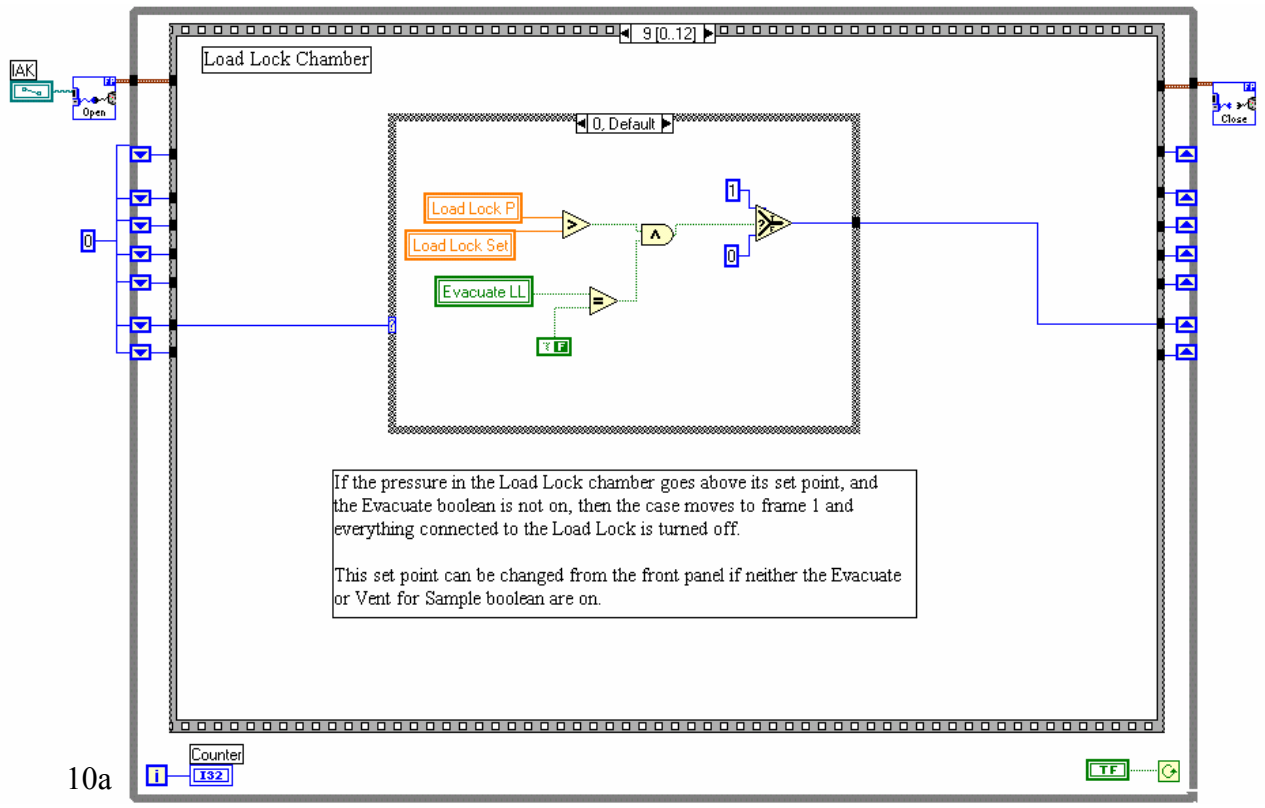

10a

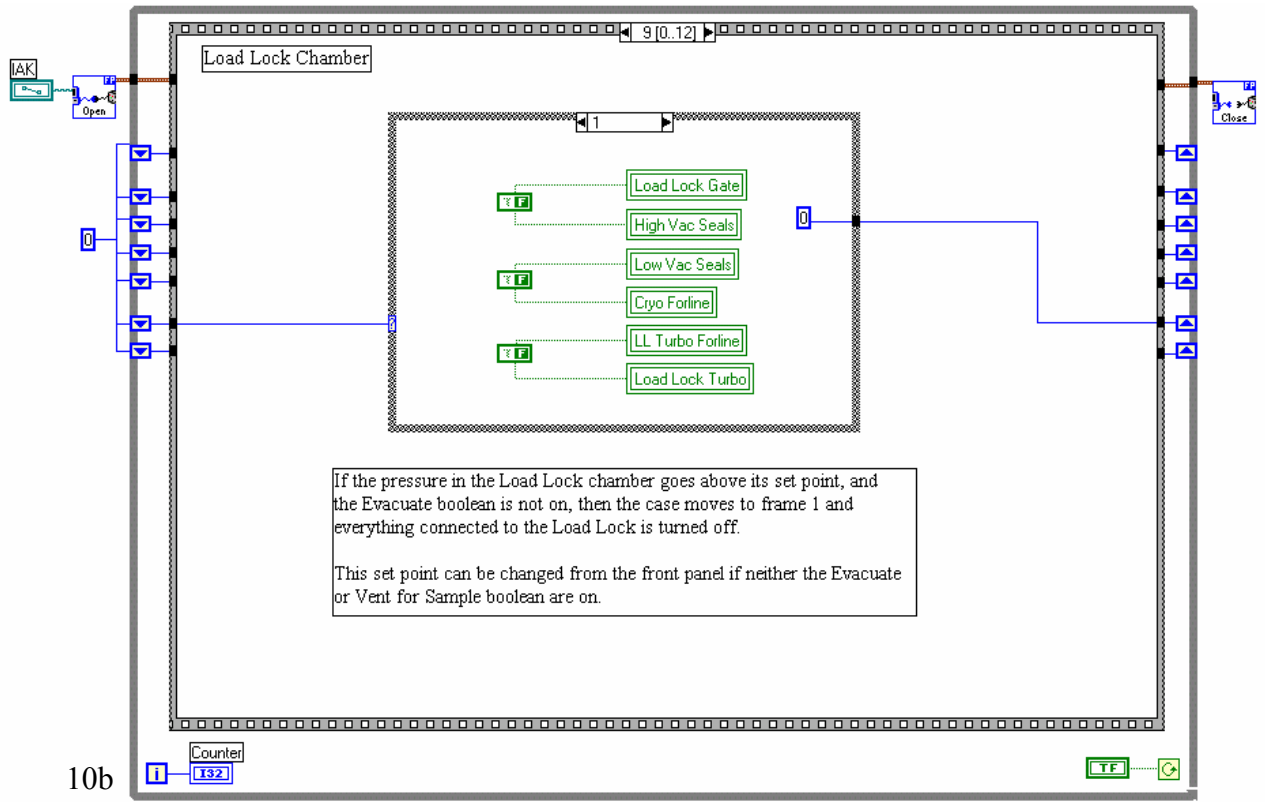

10b

Figure A.10: Load lock chamber sequence

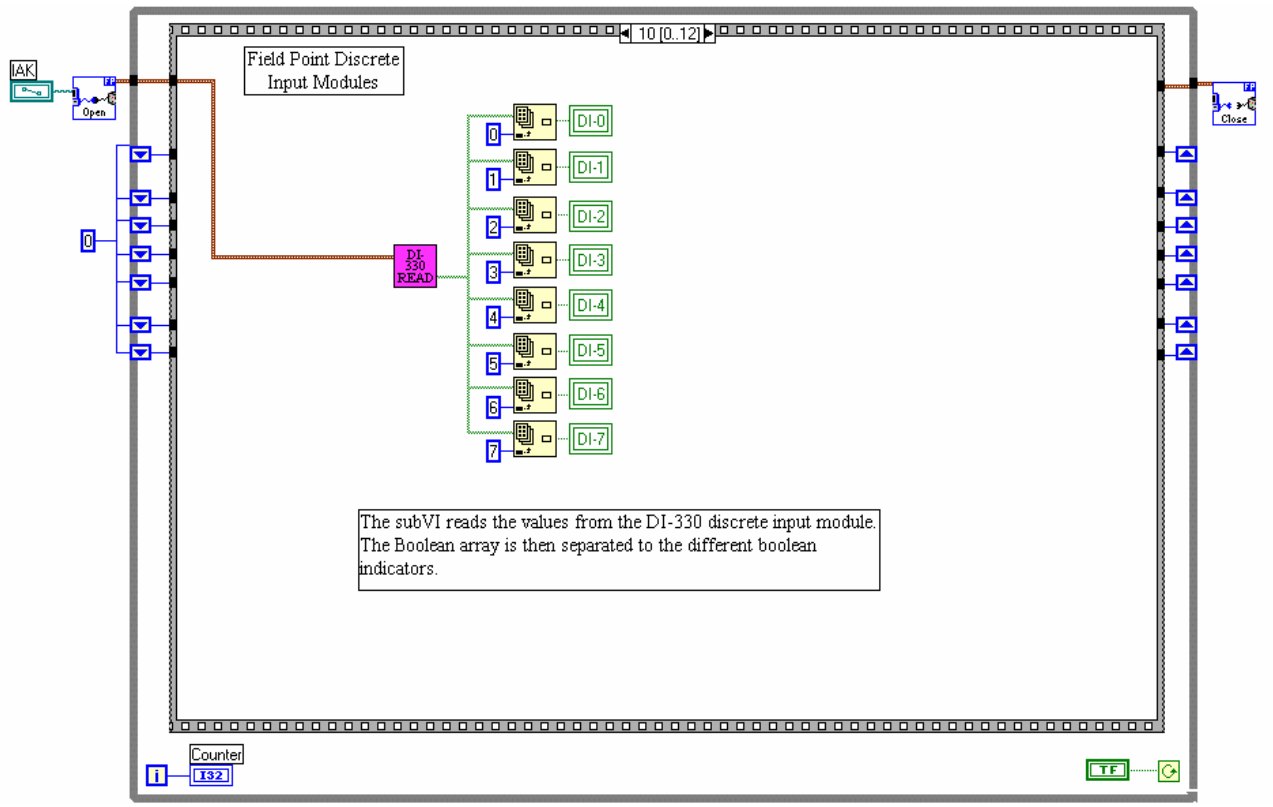

Figure A.11: Information received from discrete input modules

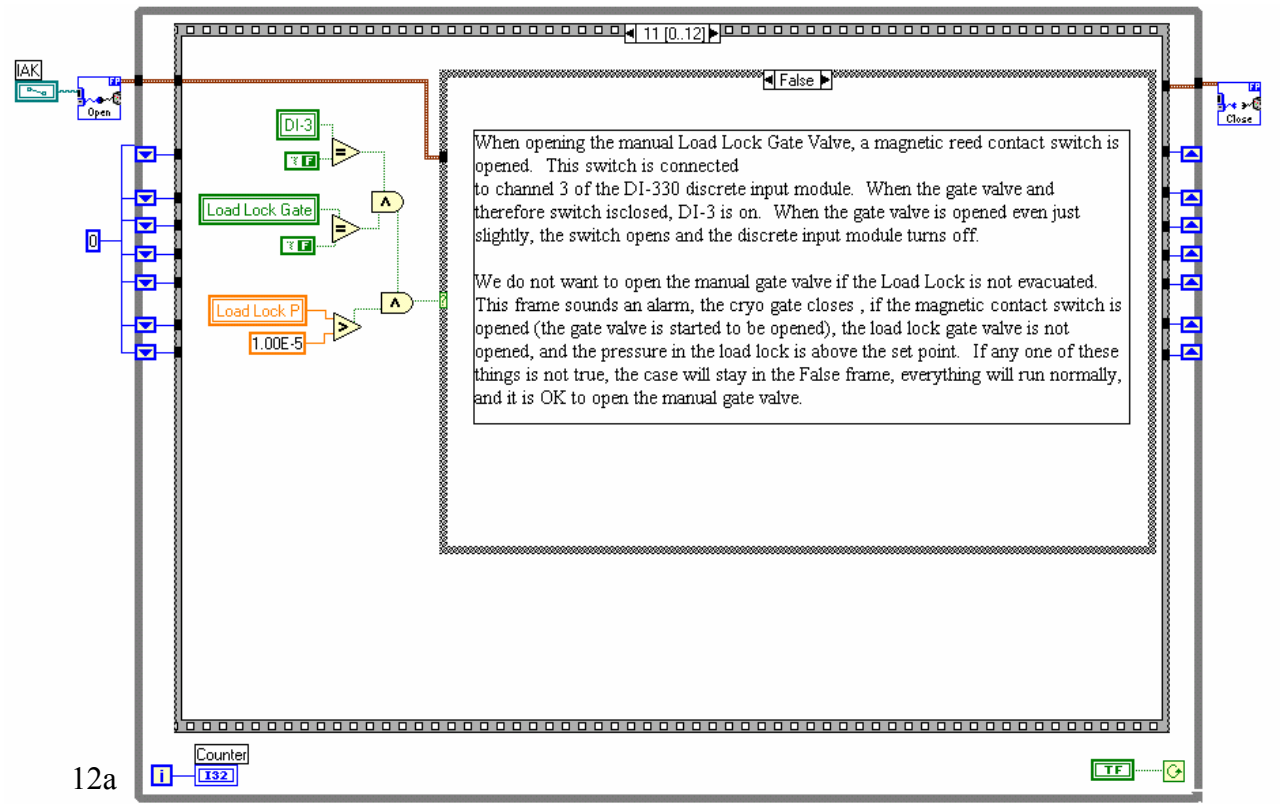
IAK
Open
11 [0..12]
False
DI-3
Load Lock Gate
Load Lock P
1.00E-5
0
When opening the manual Load Lock Gate Valve, a magnetic reed contact switch is opened. This switch is connected to channel 3 of the DI-330 discrete input module. When the gate valve and therefore switch isclosed, DI-3 is on. When the gate valve is opened even just slightly, the switch opens and the discrete input module turns off.
We do not want to open the manual gate valve if the Load Lock is not evacuated. This frame sounds an alarm, the cryo gate closes , if the magnetic contact switch is opened (the gate valve is started to be opened), the load lock gate valve is not opened, and the pressure in the load lock is above the set point. If any one of these things is not true, the case will stay in the False frame, everything will run normally, and it is OK to open the manual gate valve.
Close
Counter
I32
TF

12a

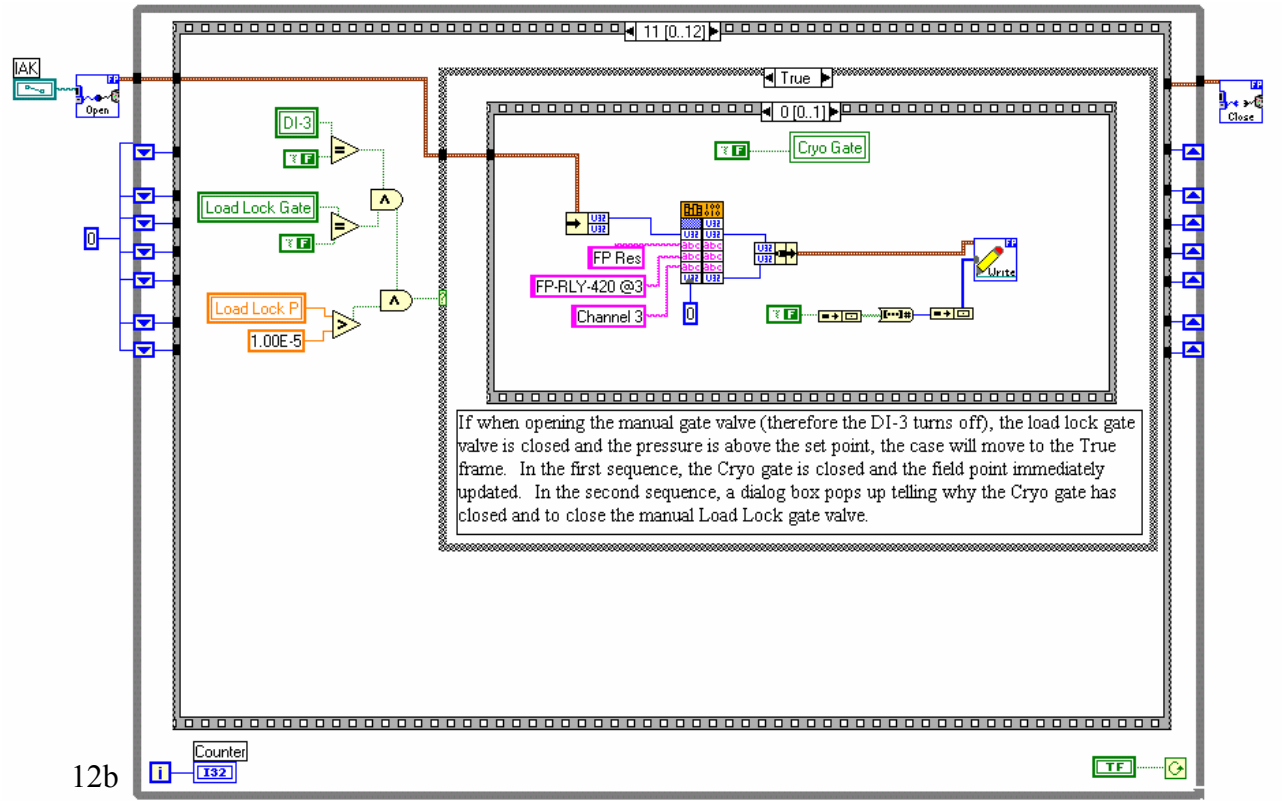
IAK
Open
11 [0..12]
True
0 [0..1]
DI-3
Load Lock Gate
Load Lock P
1.00E-5
0
Cryo Gate
FP Res
FP-RLY-420 @3
Channel 3
0
Write
If when opening the manual gate valve (therefore the DI-3 turns off), the load lock gate valve is closed and the pressure is above the set point, the case will move to the True frame. In the first sequence, the Cryo gate is closed and the field point immediately updated. In the second sequence, a dialog box pops up telling why the Cryo gate has closed and to close the manual Load Lock gate valve.
Close
Counter
I32
TF

12b

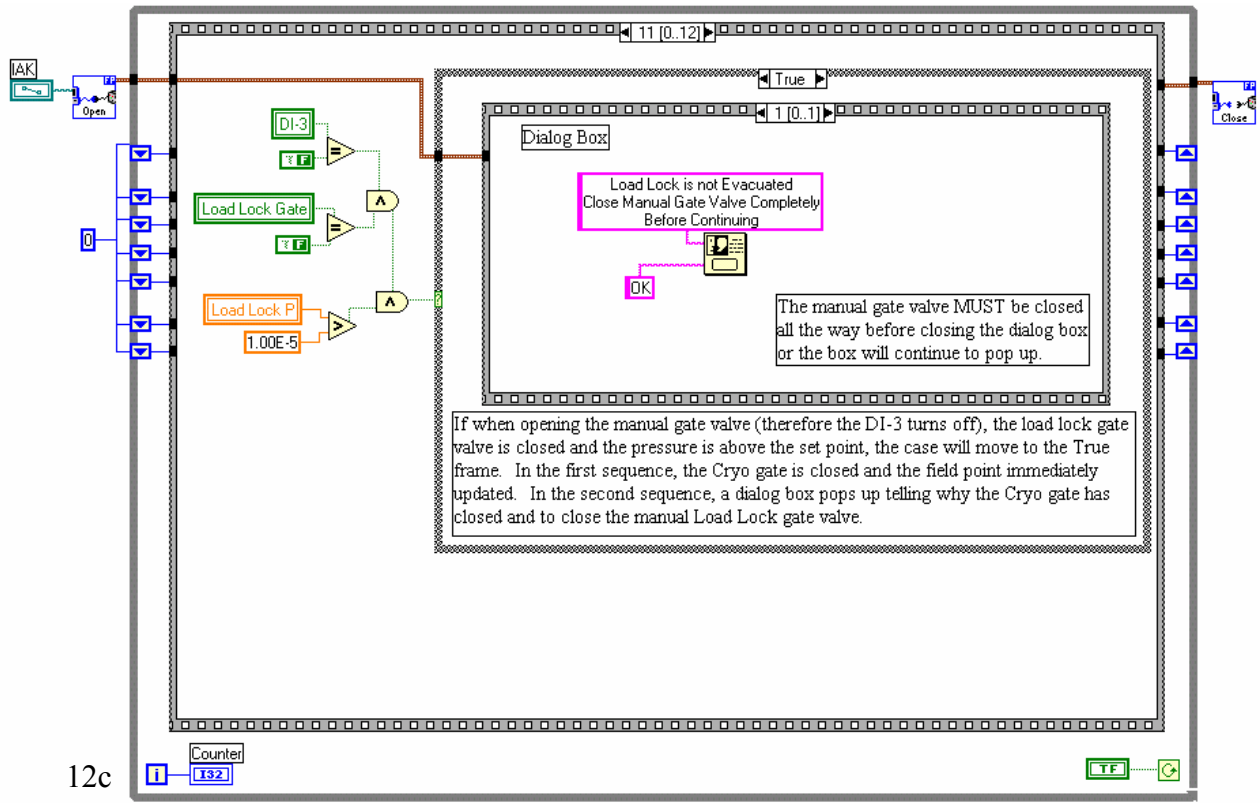

Figure A.12: Load lock manual gate alarm

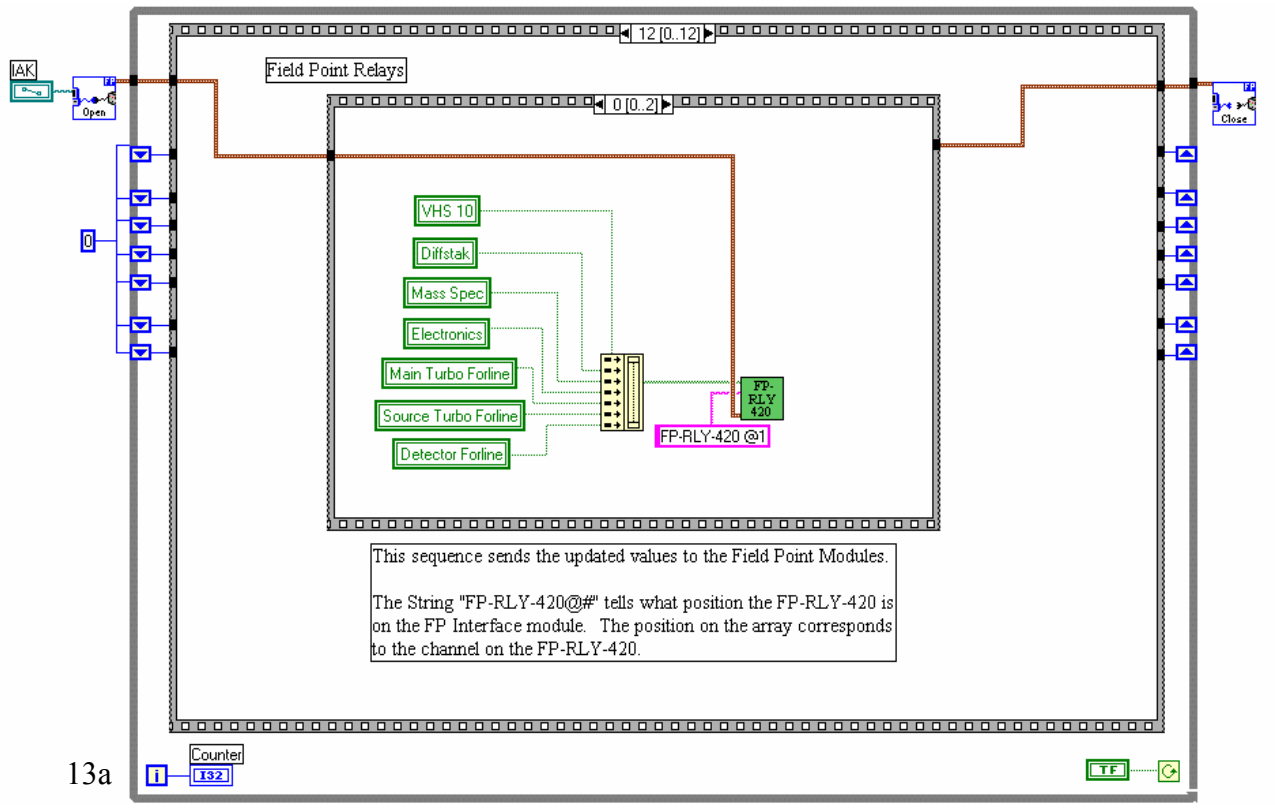
IAK
Open
Field Point Relays
12 [0..12]
0 [0..2]
0
VHS 10
Diffstak
Mass Spec
Electronics
Main Turbo Forline
Source Turbo Forline
Detector Forline
FP-RLY 420
FP-RLY-420 @1
Close
This sequence sends the updated values to the Field Point Modules.
The String "FP-RLY-420@#" tells what position the FP-RLY-420 is on the FP Interface module. The position on the array corresponds to the channel on the FP-RLY-420.
Counter
I32
TF

13a

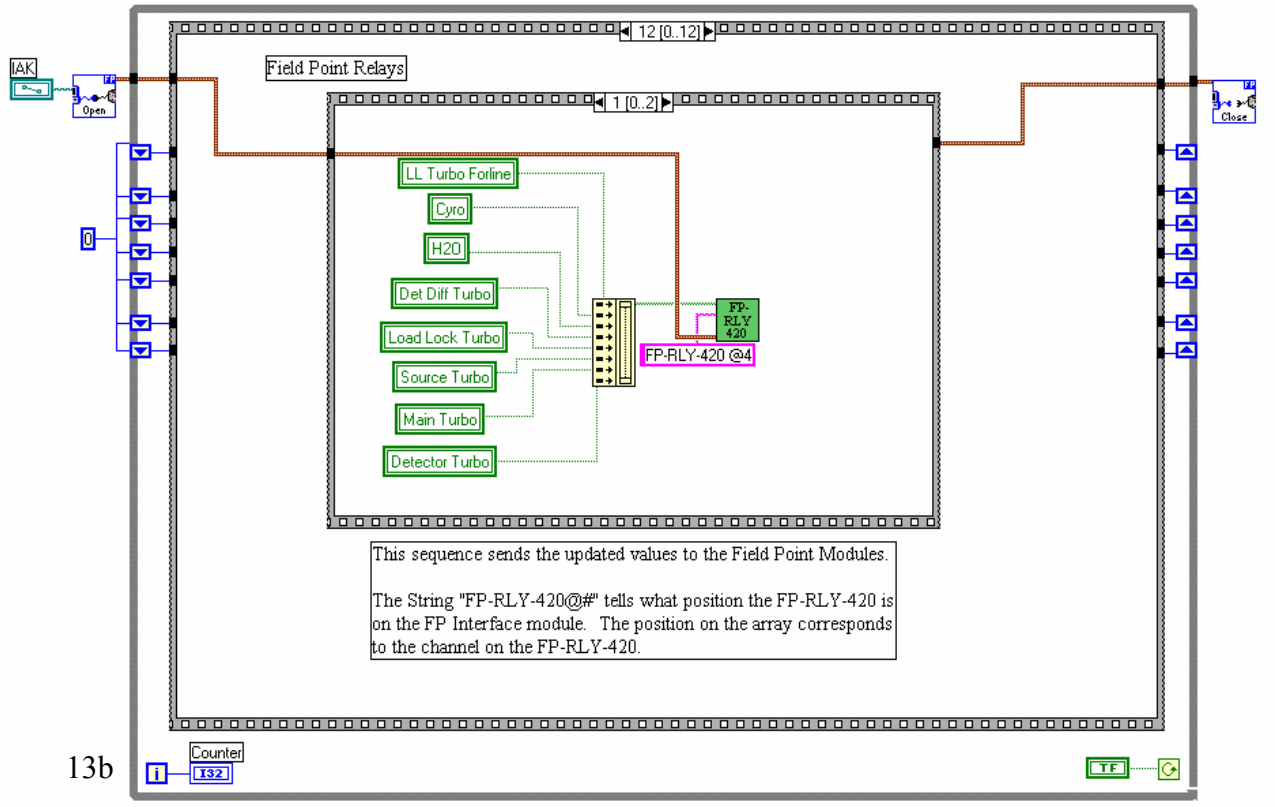
IAK
Open
Field Point Relays
12 [0..12]
1 [0..2]
0
LL Turbo Forline
Cyro
H2O
Det Diff Turbo
Load Lock Turbo
Source Turbo
Main Turbo
Detector Turbo
FP-RLY 420
FP-RLY-420 @4
Close
This sequence sends the updated values to the Field Point Modules.
The String "FP-RLY-420@#" tells what position the FP-RLY-420 is on the FP Interface module. The position on the array corresponds to the channel on the FP-RLY-420.
Counter
I32
TF

13b

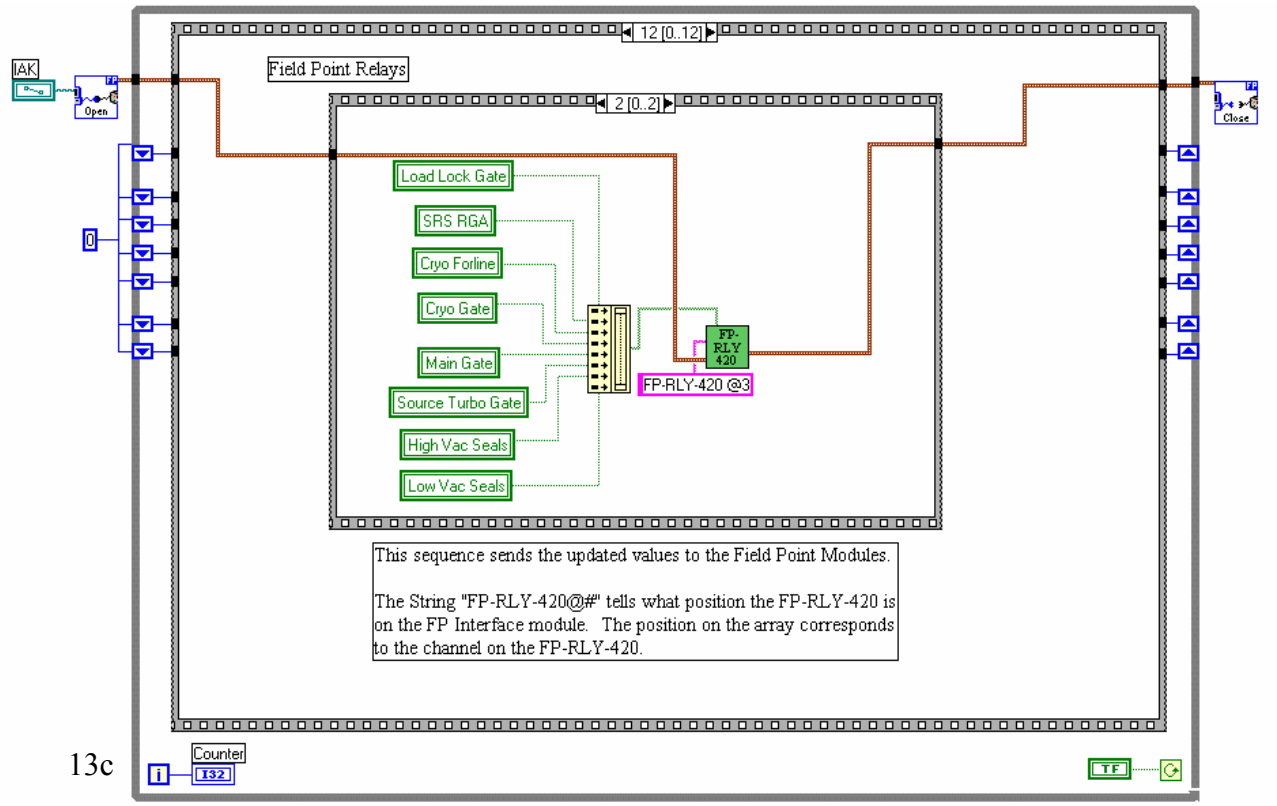

Figure A.13: Field point relay status updated

Vita

Born to Edward and Susan Westfall in 1977, Gwen grew up in Grafton, West Virginia with her younger sister, Sheila. Upon graduation from Grafton High School in 1996, she attended Radford University in Virginia. In July of 1999, Gwen was married to Paul Davis and graduated with a Bachelor of Science degree in Chemistry the following May. Gwen and Paul then moved to Blacksburg, Virginia where she entered the graduated program in the Chemistry Dept at Virginia Tech. Their son, Jacob, was born in October 2002.